The Egyptian Journal of Remote Sensing and Space Sciences 26 (2023) 861–880

Contents lists available at ScienceDirect

The Egyptian Journal of Remote Sensing and Space Sciences

journal homepage: www.sciencedirect.com

Research Paper

Trading greens for heated surfaces: Land surface temperature and perceived health risk in Greater Accra Metropolitan Area, Ghana

Ronald Reagan Gyimah [a,1], Clement kwang [a,1,*], Raymond Agyepong Antwi [b,1], Emmanuel Morgan Attua [a,1], Alex Barimah Owusu [a,1], Eric Kofi Doe [a,1]

[a] Department of Geography and Resource Development, University of Ghana, Legon, Accra, Ghana
[b] Department of Urban Forestry and Natural Resources, Southern University and A&M College, USA

ARTICLE INFO

Keywords:
Temperature
Urban built-up environment
Land cover change
Vegetation cover
Urban heat island
Urbanization
GAMA

ABSTRACT

The unsustainable expansion of cities is generating urban heat islands (UHIs) by exchanging (trading) vegetation cover (green) for built impervious surfaces which is associated with heat-related health risks, globally. This phenomenon is exacerbated by climate change and anthropogenic activities like urban population growth, particularly in African cities. This study explores the spatio-temporal trends of land surface temperature (LST), land use land cover (LULC) and their economic and health risks in the Greater Accra Metropolitan Area (GAMA) of Ghana, from 1991 to 2021. We extracted LST/LULC information from Landsat datasets to perform change analysis, alongside an online survey across 56 communities on how LST relates to economic and human health risks perceptions of residents. The results show urbanization of GAMA is trading greens for heated surfaces, impacting communities' health risks. While the built environment grew (8.6%), the vegetation cover declined (2.5%) and the mean LST rose (0.8°C) in 25 years. A 30°C LST corresponds to the point of inflexion of exchanging green vegetative cover for heated built surfaces. The forest community of Kisseman, the populous community of Dansoman and the harbour city of Tema corresponded to the first, fourth and fifth LST quintiles, changing at −0.05°C, 0.06°C and 0.164°C per year. The common health risks include discomfort from heavy sweating, headaches, dehydration, thirst and skin rashes. These results call for climate action and green spatial planning through urban forestry and environmentalism in GAMA. For urban resilience and sustainable cities, we advocate green-cooling multi-purpose housing, roads, and industrial infrastructure.

1. Introduction

With rapidly expanding urban areas, land use land cover change (LULCC) effects on urban surface temperatures and human health consequences are becoming increasingly significant issues (Jenerette et al., 2016, Chen et al., 2022). The global rise in average land surface temperatures (LST) is expected to strike urban communities more harshly due to population growth and Urban Heat Islands (UHIs) in cities (Fu and Weng, 2016; IPCC, 2021; Park et al., 2021). Climate Change (CC) in rapidly urbanizing cities triggers UHIs, economic and health effects (Halder et al., 2021; Imhoff et al., 2010). The immediate health risks of environmental hazards like UHIs are common in poor homes and neighbourhoods of heavily populated cities (Songsore and McGranahan, 2012; Das and Das 2020). Globally, the common health impacts of UHIs include heat exhaustion, general discomfort, respiratory difficulties, heatstroke and other heat-related morbidities and mortalities (Avashia et al., 2021; Halder et al., 2021). Urban heat island (UHI) occurs when urbanized areas experience warmer temperatures than nearby rural areas (Fu and Weng, 2016; Meyers et al., 2020). The phenomenon is akin to trading greens (vegetative spaces) for heated surfaces when building impervious surfaces. UHI often happens when natural vegetation (green) cover is replaced by dense concentrations of man-made heat-absorbing materials such as concrete buildings, tared and asphalt roads, iron roofing sheets, block/concrete pavements and other impervious surface build-ups in city development process (urbanization) (Sun et al., 2021; Zhou et al., 2018). These impervious materials absorb and emit heat energy that increases LST, contributing to a general rise in atmospheric air temperature (airT) and global warming (Kim and Brown, 2021; Meyers et al., 2020). In some instances, the removal of green spaces for heated surfaces exacerbates extreme heat events (EHEs) of

* Corresponding author.
E-mail address: ckwang@ug.edu.gh (C. kwang).
[1] Authors contributed equally to the research and manuscript.

https://doi.org/10.1016/j.ejrs.2023.09.004
Received 11 August 2022; Received in revised form 18 September 2023; Accepted 24 September 2023
Available online 7 October 2023

greater than 40.6ºC (Meyers et al., 2020; Nangombe et al., 2019; Chen et al., 2022).

LST is defined as the radiative energy released by various types of impervious materials that absorb and release heat within 1.2 m above ground (Fu and Weng, 2016; Meyers et al., 2020). LST and airT were terms used interchangeably in the IPCC 2021 report. According to IPCC (2021), the periods of 2001–2011 and 2011–2020 globally, experienced warmer airT by 0.99ºC (0.84–1.10 °C) and 1.09ºC (0.95–1.20 °C) respectively. The increase in airT is expected to reach 1.5-2ºC or more by 2050 (IPCC, 2021). Easterling et al. (1997) projected Africa to experience a 3-5ºC rise in mean airT measured at 1.5 m above the surface of the ground, by the end of the 21st century. Ringard et al. (2016) reported similar trends in West Africa. These increased temperatures are higher than those observed in the pre-industrial era of 1850–1900. The rise of LST and airT is attributed to the great increase in anthropogenic activities (Anthropocene) which is threatening planetary boundaries through climate change (IPCC, 2021; Rockström et al., 2009; Quan et al., 2022).

The urban population of Ghana grew by 56% within the period between 1950 and 2018, mainly in the city of Accra and Kumasi (DESA-UN, 2018; Ampim et al., 2015). Human population growth is impacting LULCC in the cities. The human population growth occasions rapid expansion of urban built-up areas characterized by urban sprawl, economic and health risks (Ampim et al., 2015; Krehbiel et al., 2016; Saviour Mantey et al., 2014). However, literature on the relationship between LULCC, UHIs measured in terms of LST and their associated economic and health risks implications for the city dwellers in Ghana is rare. Despite studies on extreme weather events particularly in low-income communities (Wilby et al., 2021; Kayaga et al., 2021), few have drawn the linkage to health risks (Jenerette et al., 2016; Codjoe et al., 2020). For instance, Jenerette et al., (2016) observed the LST, LULCC, LST and health risk nexus in Pheonix (Arizona, USA) that provided evidence for critical look at heat vulnerability and city planning in that state. However, this type of evidence is patchy in GAMA and thus hinders green spatial planning for health benefits it the city. This study, therefore, seeks to explore the linkages of LULCC, LST and its perceived health risk on residents in the Greater Accra Metropolicatan Area (GAMA). According to Gonzalez-Trevizo et al. (2021) and Chapman et al. (2017), there is overly concentrated literature on LULCC/UHIs in most advanced parts of the world while such knowledge in developing countries remains less known. This dearth of information exists in the Greater Accra Metropolitan Area (GAMA) of Ghana where city dwellers are becoming potentially vulnerable to health risks due to increasing LULCC and UHIs linkages (Acheampong, 2019; Ampim et al., 2015). The situation of GAMA becomes scarier considering the inability of the city planners and health systems to develop contingency plans to address current and future UHIs (Johnson et al., 2012). Assessing the trends of LST and to suggest ways to reduce its severe human health risks are concerns for city dwellers, researchers and world policymakers. Unearthing the trends of LST/LULCC as scientific evidence is useful for advocating the need for building climate-resilient and liveable cities (UN-HABITAT, 2020, Ampim et al., 2015; Puplampu and Boafo, 2021). It is relevant for regional and urban spatial planners and for providing heat-related health risks information, adaptation and coping strategies against high LST and UHIs. Since public health risks of UHI epitomized by remotely sensed LST data have been marginal in Ghana's research space, the current study seeks to explore the phenomenon of trading green spaces for heated surfaces (UHI) in GAMA, from 1991 to 2021. Specifically, the study seeks to determine the nexus between urban LST, built-up expansion and vegetation loss changes and their health implications for urban community dwellers in GAMA.

2. Methods

2.1. Study area

The study was conducted in GAMA, which lies within the coastal savannah ecological and dry equatorial climatic zones (Fig. 1). It is located along the southern coast of the Gulf of Guinea, covering a total land area of 1,524.99 km^2. GAMA is a low-lying area (below sea level) with an average annual rainfall of about 730 mm. The annual average temperature of the area is 25 °C with monthly mean temperatures ranging from 22 °C to 33 °C (Wemegah et al., 2020). Coastal lands (wetlands and dunes), shrublands and grassland constitute the major vegetation zones of GAMA.

The GAMA spans 30 Metropolitan, Municipal and Districts (MMDA) with a total population of 5,454,959. According to the Ghana Statistical Service, (2021), males constitute 48.97% whereas females form 51.03% of the population in 2020. GAMA is a relatively high-income city, dubbed the "*economic hub*" of the Greater Accra Region and the entire country (Songsore et al., 2006). GAMA was chosen for this study due to the urban milieu and ecological dynamics it presents. For instance, there is high demand for land for housing, road expansion and business development to create employment centres and tourism among other economic and social infrastructure projects (Oduro et al., 2015).

2.2. Study design

A hybrid approach of spatio-temporal analytical techniques involving remote sensing and geographic information systems and a semi-structured questionnaire survey of 56 communities involving 103 participants was used. The methodological approach is summarized in Fig. 2.

2.3. Study data- satellite datasets acquisition and pre-processing

As shown in Fig. 2, remotely sensed Landsat datasets were downloaded from the US Geological Survey (USGS) website (http://earthexplorer.usgs.gov) and pre-processed to determine the NDVI and their respective LST. The metadata of the Landsat data series is provided in Table 1.

The pre-processing of the Landsat images was done to suppress distortion or enhance important features for further processing and analysis (Vision, 1993). The image pre-processing includes radiometric and atmospheric corrections, subsetting and stacking selected bands to form composite images. In this study, the digital numbers (DNs) of the features were converted to Top of Atmosphere (TOA) radiance using equation Eq.1 (Adeyeri et al., 2017).

$$L_\lambda = M_L Q_{cal} + A_L \quad (1)$$

where:

L_λ is the TOA measured in Watts/ m^2 *srad *μm. M_L and A_L are band multiplicative and additive rescaling factors, respectively indicated in the metadata file of the Landsat data, and Q_{cal} is quantized and calibrated digital number (DN).

After converting DNs to TOA, image calibration was performed with dark object subtraction (DOS) equation to get the images in surface reflectance using equation Eq.2.

$$R_c = R_s + R_{si} \quad (2)$$

where:

R_c is an atmospherically rectified image, R_s is the TOA and R_{si} is given by the formula Mean Rw–(2*Standard Deviation Rw), where Rw is defined as the spectral value being considered as an offset. The DOS method has the advantage of producing an atmospherically corrected image (Kane et al., 2016).

2.4. LULC categorizations and change detection analysis

LULC analysis is an essential tool for understanding and managing changes within the urban spaces (Xu et al., 2022). Image classification and LULC categorizations were performed after the pre-processing. The image classification automatically grouped the pixels into their

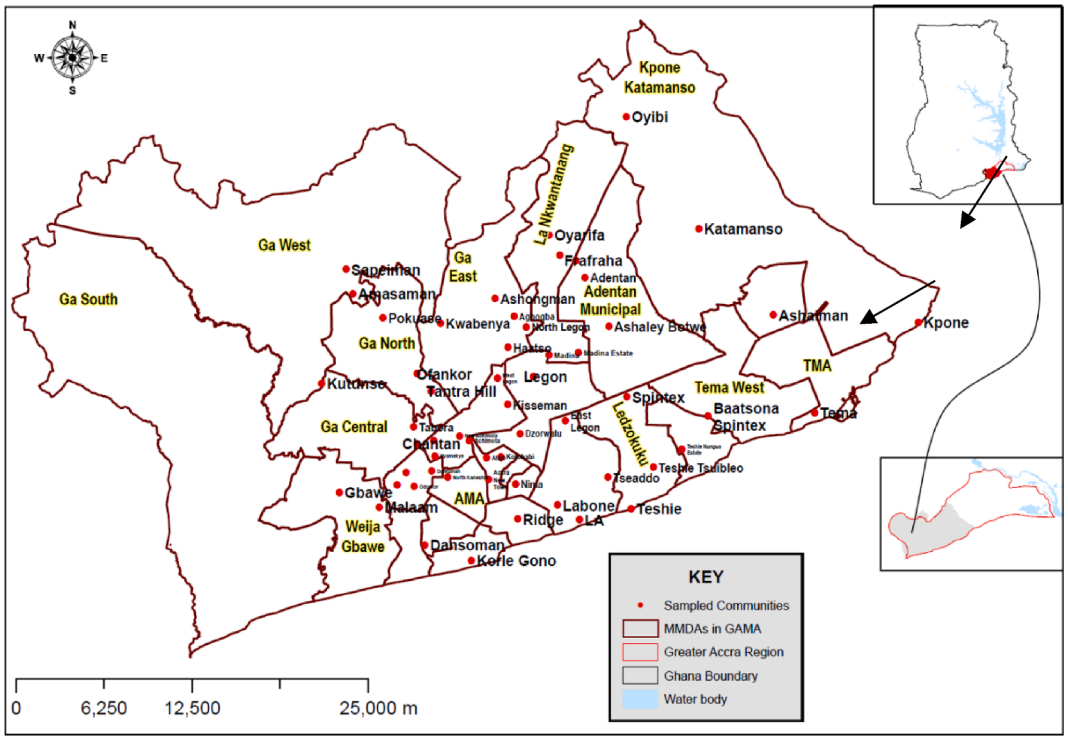

Fig. 1. Study Area Map showing MMDA boundaries and sampled communities.

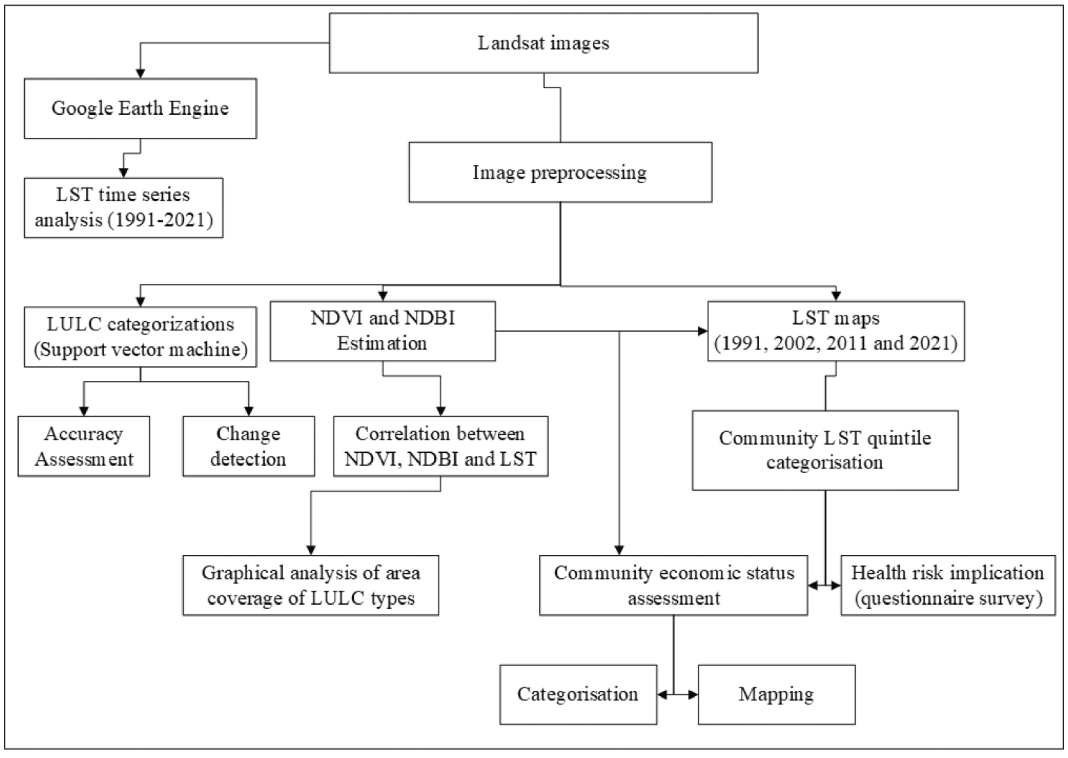

Fig. 2. Methodological Workflow.

respective land cover types with the main objective of creating thematic LULC maps (Saha et al., 2021). The support vector machine (SVM) is a non-parametric classifier that produces superior results relative to the maximum likelihood classifier, neural network classifier and decision tree classifier (Kavzoglu and Colkesen, 2009; Huang et al., 2002). The SVM algorithm provides higher stability and accuracy and these were the main reasons it was used in this study. Authors that used SVM in LULC studies include Liu et al., (2022); Nyamekye et al., (2021); Tian et al., (2020); Shao and Lunetta, (2012). The GAMA LULC maps were classified into built-up, waterbody and vegetation classes using the SVM algorithm in QGIS software. The descriptions of the LULC classes are explained (Table 2).

Table 1
Metadata of Landsat data series.

Path/ Row	Sensor	Scene ID	Acquisition date	Time (GMT)	Season
193/056	Landsat 4 TM	LT41930561991010XXX03	1991-01-10	09:40:09	Dry
193/056	Landsat 7 ETM+	LE71930562002024EDC00	2002/01/24	10:04:20	Dry
193/056	Landsat 7 ETM+	LE71930562011017ASN00	2011-01-17	10:09:00	Dry
193/056	Landsat 8 OLI &TIRS	LC81930562021004LGN00	2021/01/04	09:33:24	Dry

Table 2
LULC class categorization and description.

LULC type	Description
Vegetation	Grassland, dense forest and urban vegetation such as forest reserves, parks, lawns and vegetated recreational areas
Built-up	Urbanized and industrial areas, open lands such as barren land and wasteland
Waterbody	Wetlands, rivers, lakes, canals, lagoons, riparian and ponds

The spatio-temporal changes in the LULC types between two different years were analyzed using the algebra-based change detection approach. The algebra-based approach was chosen because it was easy to implement and detect different scales of changes in the LULC types (Afaq and Manocha, 2021). Post-classification image differencing method was used to determine the changing pattern and acreage for each LULC type from 1991 to 2021. The post-classification image differencing method assesses the spatial variation in the two images by analyzing the intensity of each pixel colour (Minu and Shetty, 2015). The change in acreage for each LULC type was further analyzed using Microsoft Excel to explore the trends and patterns of the spatio-temporal changes. The following equations were applied in determining the change in LULC types in percentage and rate of change in LULC.

$$ChangeinLULC(\text{ha}) = \frac{LULC_{Currentyear} - LULC_{Pastyear}}{LULC_{Pastyear}} \quad (3)$$

$$\%ChangeinLULC(ha) = \frac{LULC_{Currentyear} - LULC_{Pastyear}}{LULC_{Pastyear}} x100\% \quad (4)$$

$$RateofChangeinLULCperyear = \left[\left(\frac{LULC_{Currentyear} - LULC_{Pastyear}}{LULC_{Pastyear}}\right)x100\%\right] \tilde{A}\cdot 30year \quad (5)$$

2.5. Accuracy assessment

An accuracy assessment was performed on each of the LULC category maps to determine their level of accuracy in predicting each LULC type. Five hundred and thirty (530) accuracy assessment points were generated for each LULC category map by using the stratified random sampling technique (Ranagalage et al., 2019) in ArcGIS software. Google Earth historical images were then used as reference data for determining the truth points for the 530 accuracy assessment points of 1991, 2002, 2011 and 2021 LULC maps. The confusion matrix was created by using the accuracy assessment points for each of the LULC maps in order to determine the accuracies (user's accuracy, producer's accuracy and overall accuracy) and Kappa coefficient. The user's accuracy accounts for commission errors while the producer's accuracy deals with omission errors (Ranagalage et al., 2019). The kappa coefficient is used in remote sensing image classifications to express the accuracy of LULC categorized maps (Foody, 2020; Xu et al., 2022).

2.6. Derivation of NDBI and NDVI from Landsat images

The Normalized Difference Built-up Index (NDBI) and Normalized Difference Vegetation Index (NDVI) were used to establish the nexus of LST, built-up expansion and vegetation cover loss, following Jenerette et al., (2016) and Guha et al., (2021). NDBI denotes built-up areas which correlate positively with LST. NDVI reflects vegetation greenness and is inversely related to LST. In this study, the NDBI and NDVI of 1991, 2002, 2011 and 2021 were estimated using atmospherically rectified Landsat series of 30 m spatial resolution. We calculated the NDBI and NDVI following Jones and Vaughan, (2010), Huang et al., (2021) and Zheng et al., (2021) using Eq. (6) and Eq. (7) respectively.

$$NDBI = \frac{ShortwaveNearinfrared - Nearinfraredband(SWNIR - NIR)}{ShortwaveNearinfrared + Nearinfraredband(SWNIR + NIR)} \quad (6)$$

$$NDVI = \frac{(Near - infraredband - Redband)}{(Near - infraredband + Redband)} \quad (7)$$

Both NDVI and NDBI values range from −1 to + 1. Positive NDVI values indicate vegetated areas, while negative values are non-vegetated areas. NDVI value close to 0.00–0.25 indicates a bare surface, 1.00–0.99 for water and 0.30–1.00 for vegetation (Jones and Vaughan, 2010). High positive NDVI values show dense vegetation cover such as forest (Huang et al., 2021). Positive NDBI values depict built urban land areas, and negative values represent non-built urban land areas (Zheng et al., 2021).

2.7. Retrieval of land surface temperature for 1991, 2000, 2010 and 2020

Retrieving the LST data from NDVI followed a mono-window algorithm that estimates LST from Landsat thermal bands (Kumari et al., 2021, Kafy et al., 2021). This involves four steps; (1) DN-spectral radiance conversion, (2) converting spectral radiance to brightness temperature (Zhao et al., 2021), (3) application of atmospheric correction on the thermal bands using dark object subtraction (4) a proportion of vegetation to correct emissivity and (5) estimating LST (Yao et al., 2021) as illustrated in the steps below.

In step 1, the DN values of thermal bands were converted to spectral radiance using eq. (6).

$$L_\lambda = L_{min} + (L_{max} + L_{min}) \times \frac{DN}{255} \quad (8)$$

where, L_λ is the spectral radiance; For Landsat 5; L_{min}= 1.238; L_{max} = 15.30; for Landsat 7; L_{min} = 0.0; L_{max}= 17.04; For Landsat 8; L_{min}= 0.10033; L_{max} = 22.00180 (Kafy et al., 2021).

After converting the radiometric correction, the spectral radiance was changed to the atmosphere brightness temperature (T_B) in Kelvin with eq. (9).

$$T_B = \frac{K_2}{\ln((K_1/L_\lambda)+1)} \quad (9)$$

where, K_1 is Calibration constant 1; K_2 Calibration constant 2; For Landsat 4, K_1 = 671.62; K_2=1284.30; For Landsat 7, K_1 = 666.09; K_2=1260.56; For Landsat 8, K_1 = 480.88; K_2=1201.14 (Kafy et a l., 2021; Zhao et al., 2021).

We converted LST measured in Kelvin to degree Celsius (C) using Eq. (10).

$$T_B(C) = T_B(K) - 273.15 \quad (10)$$

This enabled estimation of the LST from the T_B in degree Celsius (C) using the following equation Eq10.

$$LST = T_B/(1 + (\lambda \times T_B/\rho) \times \ln(\mathscr{E})) \quad (11)$$

Where, λ is wavelength of emitted radiance = 11.5 μm, ρ = 1.438 × 102mK (Kafy et al., 2021);

$$\text{Surface emissivity, } \mathscr{E} = 0.004PV + 0.986 \quad (12)$$

(Kafy et al., 2021).

$$\text{The proportion of Vegetation, } PV = (NDVI - NDVI_{min}/NDVI_{max} - NDVI_{min}) \quad (13)$$

Where $NDVI_{max}$ and $NDVI_{min}$ are highest and lowest NDVI values respectively (Kafy et al., 2021).

The approach used in estimating the LST in this study is one of the most widely used methods in determining LST using remote sensing data. Authors such as Athukorala and Murayama, 2020; Dissanayake et al., 2019; Ranagalage et al., 2019 and Simwanda et al., 2019 have successfully applied the approach in estimating LST.

2.8. Time series analysis of land surface temperature over 25 years

The aforementioned LST approach requires downloading several large Landsat data over 25 years for a time trend analysis (Ermida et al., 2020). Since LST fluctuates frequently over short periods, it necessitates the use of several Landsat datasets to estimate the long-term mean, minimum and maximum LST. Therefore, we employed Ermida et al, (2020)'s automated Google Earth Engine (GEE) java scripts, to simplify the extraction of the LST information from 341 Landsat datasets over 16 to 25 years. We then applied ordinary least square (OLS) regression to estimate the trend and the absolute (ab) change (±) in the LST over the years (n) observed. See supplementary file 1.1. The 341 Landsat dataset enabled us to cross-validate our initial LST estimates for 1991, 2000, 2010 and 2020 datasets. Pelta and Chudnovsky, (2017)'s augmented airT predicted a higher accuracy of temperature brightness (T_B) using meteorological data. We employed ERA-5 atmospheric data (supplementary file 1.1) to cross-validate our LST estimates.

2.9. Assessing the health risks of land surface temperature

We designed a semi-structured questionnaire using Google Forms and administered it online through social media platforms to conduct a cross-sectional assessment of socioeconomic and health risks of urban LST in GAMA. The questions elicited perceived risks from 103 respondents living in 56 GAMA communities. The data were analysed using STATA.

2.10. Assessing the relationship between NDVI and LST

NDVI has a direct relationship with LST even though the correlation would be negative. NDVI-LST were established using statistical software such as Excel spreadsheets. The correlation results were displayed graphically as a scatter plot chart.

Some 56 communities in the study were characterized according to their LST quintiles and income classes. Each quintile (q) corresponds to one-fifth (≃11/56) of the 56 communities as well as one-fifth (20th %) of LST estimated. This characterization was done by creating a 1 km buffer from the observed community centre and extracting the LST values within the buffer to estimate the minimum, maximum and mean LST at the community level for 1991, 2001, 2011 and 2021. This enabled a trend analysis of the community LST from 1991 to 2021. Determination of the community income class was done using the Accra Metropolitan Assembly (AMA) community income rankings as low income, middle income and high income. AMA does this classification for tax collection purposes and the main variables used in this classification are building quality, building structuring and socio-economic infrastructure available in the communities. An analysis of variance (ANOVA) and Kruskal-Wallis test of difference in community LST between the years were also conducted to determine any statistical differences in the LST estimates over the years and across income classes.

2.11. Spatial correlation of community NDVI, income status and LST in GAMA

A spatial correlation map of the community NDVI, income status and LST quintile was created using inverse difference weighting (IDW) and a raster calculator in ArcMap. It was done by coding the community NDVI as 1 = vegetation and 0 = no vegetation. The community income status was coded as 100 = low income, 200 = middle income, and 300 = high-income communities. The codes for the community LST quintiles were 1000 = very low LSTq1, 2000 = low LSTq2, 3000 = moderate LSTq3, 4000 = high LSTq4 and 5000 = very high LSTq5. These codes were interpolated using IDW and then reclassified to their corresponding codes. Each of these IDW interpolations was resampled to the same resolution of 30 m × 30 m and then layer stacked by adding them using the raster calculator tool. Our priority expectation was that high-income communities are likely to have more impervious surfaces replacing the vegetative cover. The low-income communities are likely to be more vegetative and have fewer impervious surfaces.

3. Results

3.1. Relationship of land surface temperature change, built-up expansion and vegetation cover loss

3.1.1. Spatio-temporal trends of annual and seasonal land surface temperature in GAMA

The survey reveals that most of the respondents (93%) believe that there is a surge in GAMA LST, attributable mainly to climate change. The physical evidence for the temperature rise is presented in Fig. 3. Fig. 3 illustrates the spatio-temporal distribution of the observed LST as of 1991 (Fig. 3a), 2002 (Fig. 3b), 2011 (Fig. 3c) and 2021 (Fig. 3d) based on the four dry seasons Landsat datasets. The highest maximum LST of 49.0°C (mean = 33°C) occurred in 2021 and the lowest maximum ever experienced, 30.0°C (mean = 27°C), took place in 1991. The mean LST increased by 6°C (22.2%) from 27°C to 33°C during the period.

Table 3 shows the annual mean, minimum and maximum LST statistics were 31.9°C, 27.3°C and 33.9°C, respectively, based on the 341 Landsat time series dataset. The dry (Dec-Mar) season mean LST was 32.6 ± 1.4°C. While the wet season 1 (Apr-Jul) LST was 31.4 ± 3.3°C, it was 32.1 ± 2.2°C in the wet season 2 (Aug-Nov).

The time trends of the annual and seasonal LST are shown in Fig. 4. The annual mean LST increased at 0.03°C per year (Fig. 4a), culminating

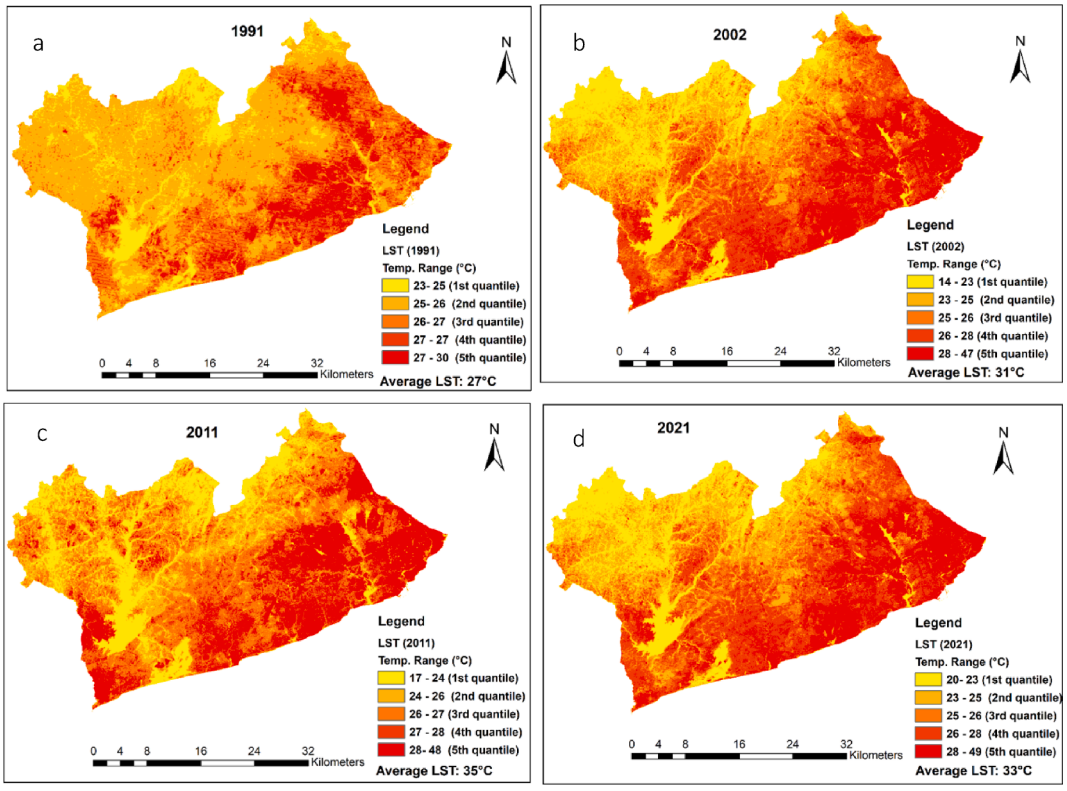

Fig. 3. Patterns of spatio-temporal land surface temperature as of January (a) 1991, (b) 2002, (c) 2011 and (d) 2021 in GAMA.

Table 3
Descriptive statistics of annual and seasonal LST in GAMA.

Variable	Period	Number of Years	Mean (°C)	Std. Dev. (°C)	Min (°C)	Max (°C)
GAMA LST (annual)	1991, 1998–2021	25	31.9	1.5	27.3	33.9
Dec-Mar (Dry season)	1991, 1999–2021	24	32.6	1.4	29.6	35.1
Apr-Jul (Wet season 1)	2000–2020*	16	31.4	3.3	26.0	37.4
Aug Nov (Wet season 2)	1998-2020†	22	32.1	2.2	27.3	35.2
Missing data in 2001, 2008–2011 (*) and 2010 (†)						

in a 0.8°C rise over 25 years. While the trend of the dry season LST was constant (Fig. 4b), it took downward and upward paths in both wet seasons 1 (Fig. 4c) and 2 (Fig. 4d).

3.1.2. GAMA LST, NDVI, NBVI and LULC change relationship

Fig. 5 shows the built environment in GAMA grew by 258.7% (849.6 km^2) at an annual rate of 8.6% in the 30 years while the vegetation cover experienced a 74.6% (846.3 km^2) decline at 2.5% per annum. The water bodies also decreased by 3.3 km^2. The built-up area increased drastically to overtake the vegetation cover after 2002 and continued to 2021 at an annual rate of 8.6%. Table 4 indicates that the accuracy of the LULC classifications was high. The overall classification accuracy was 97.4% (kappa = 0.93) for 1991 (Fig. 5a), 94.3% (kappa = 0.85) for 2002 (Fig. 5b), 94.2% (kappa = 0.88) for 2011 (Fig. 5c) and 95.8% (kappa = 0.88) for 2021 (Fig. 5d) LULC classes.

The dwindling vegetation cover and increasing built-up (heated impervious) surfaces intermediate the surge in LST change with GAMA. As shown in Fig. 6, the LST, NDVI and NBVI relationship suggests that at a mean LST greater than 30°C, the built-up area exceeds the vegetation cover and vice versa.

3.1.3. Spatial pattern of community land surface temperature in quintiles

Fig. 7 characterizes the community-level LST in quintile (q) as of January 2021. The participants (N = 103) of the survey lived in the 56 communities within GAMA as indicated by the circles and boundaries in Fig. 7. The circles represent a 1 km radius from the community centroid (GPS point). Fig. 7a depicts the general pattern of variability in the LST. In general, the mean LST (Fig. 7b) was 26.95°C (ranging from 24.53°C mean minimum to 29.48°C mean maximum) at the community level. Fig. 7c and Fig. 7d demonstrate the spatial distribution of the minimum range (19.5°C-27.4°C) and maximum range (27.1°C-47.8°C) LST for all communities respectively.

Tema was among the fifth (highest) community LSTq5 category, followed by Dansoman in the fourth (LST4q) category and Ridge in the third (LSTq3) category. Legon was in the second LSTq2 while Kisseman was among the first (lowest) LSTq category.

3.1.4. Temporal trends and changes in LST within study communities

Descriptive statistics of the temporal trends and changes in the community land surface temperature quintile (LSTq) are presented in Table 5. Tema was among the highest LSTq5 ($\leq 100^{th}$ %) of 35.0 ± 2.4°C, while Kisseman was in the lowest LSTq1 ($\leq 20^{th}$ %) at 31.0 ± 2.3°C.

Furthermore, 8a shows there was a 0.164°C rise in the mean LST per annum in Tema. This implies a 4.1°C temperature increase over the 25 years. On the contrary, Fig. 8e revealed a 0.05°C decrease in the mean

Kisseman community LST per annum, which implies a 1.2ºC increase over the 24 years.

The bar graphs in Fig. 9 exhibit variations of community-level LSTq in GAMA from 1991 to 2021 based on the four dry seasons Landsat dataset. There were upward trends in the Very high LSTq5 (Fig. 9a), High LSTq4 (Fig. 9b) and Moderate LSTq3 (Fig. 9c) quintile communities. The trends were downward in the Low LSTq2 (Fig. 9d) and Very low LSTq1 (Fig. 9e) quintile communities.

The ANOVA and Kruskal-Wallis tests of the significance of the difference in the minimum, maximum and mean LST (ºC) observed in 1991, 2001, 2011 and 2021. The mean community LST in 1991 ($\mu = 26.9 \pm 0.6$, median = 26.9), 2001 ($\mu = 26.9 \pm 1.3$, median = 27.3), 2011 ($\mu = 27.2 \pm 1.0$, median = 27.5) and 2021 ($\mu = 26.9 \pm 1.3$, median = 27.3), and were not statistically different (Kruskal-Wallis $\chi^2 = 5.453$, p-value = 0.142, df = 3). Concerning the minimum community LST in 1991 ($\mu = 25.5 \pm 0.63$, median = 25.2), 2001 ($\mu = 23.5 \pm 1.8$, median = 23.8), 2011 ($\mu = 24.2 \pm 1.6$, median = 24.4) and 2021 ($\mu = 23.5 \pm 0.63$, median = 23.8), the test showed at least one of the rank sums was statistically different from the others (Kruskal-Wallis $\chi^2 = 48.419$, p-value = 0.000, df = 3). Similarly, a significant statistical difference was observed for the maximum community LST (Kruskal-Wallis $\chi^2 = 81.845$, p-value = 0.000, df = 3) for 1991 ($\mu = 28.1 \pm 0.5$, median = 28.1), 2001 ($\mu = 30.0 \pm 2.7$, median = 29.7), 2011 ($\mu = 29.4 \pm 1.2$, median = 29.0) and 2021 ($\mu = 30.0 \pm 2.7$, median = 29.7).

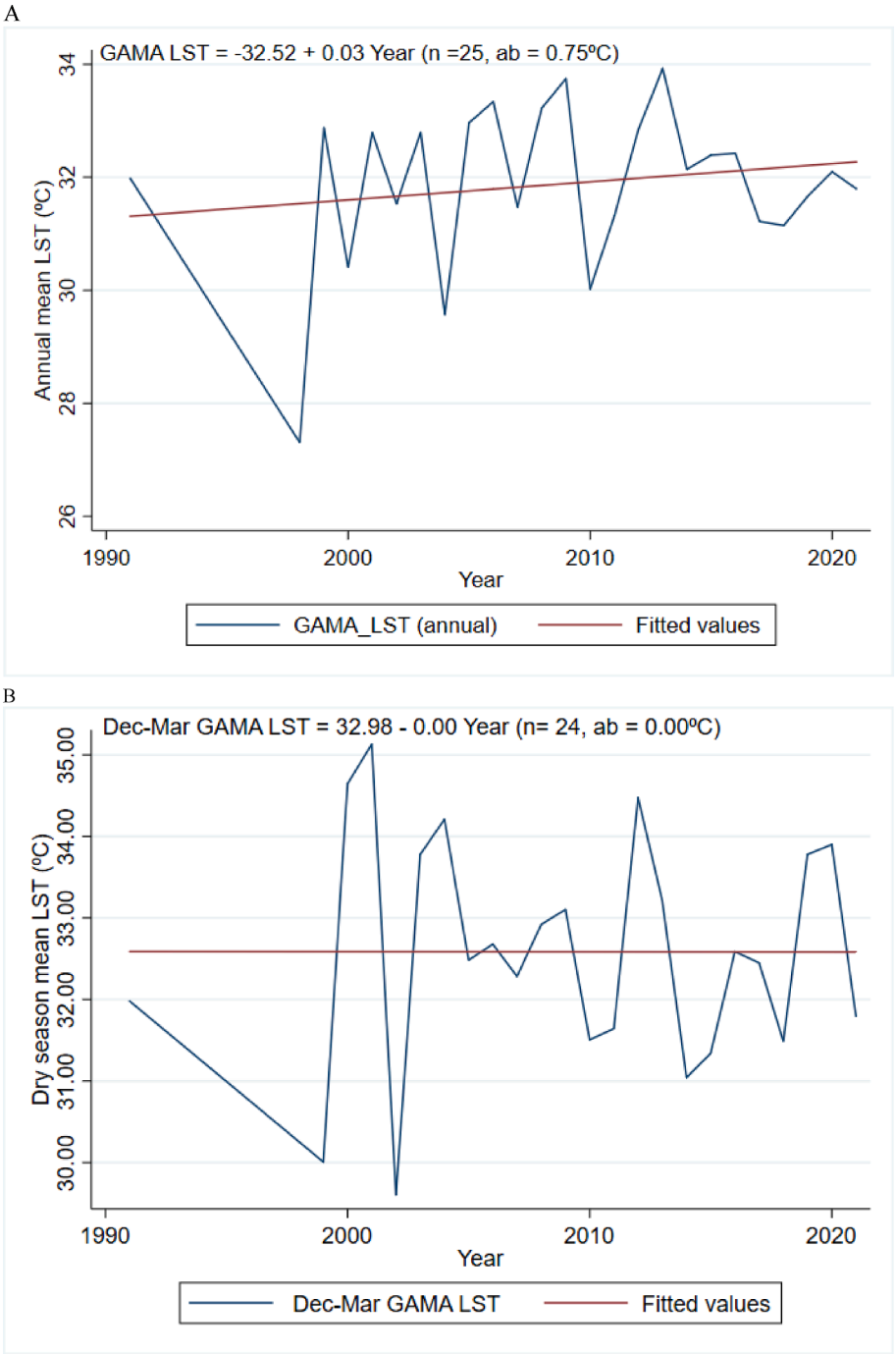

Fig. 4. Trends of annual (a) and dry season (b), wet season 1 (c) and wet season 2 (d) LST in GAMA (n = number of years; ab = absolute change ±).

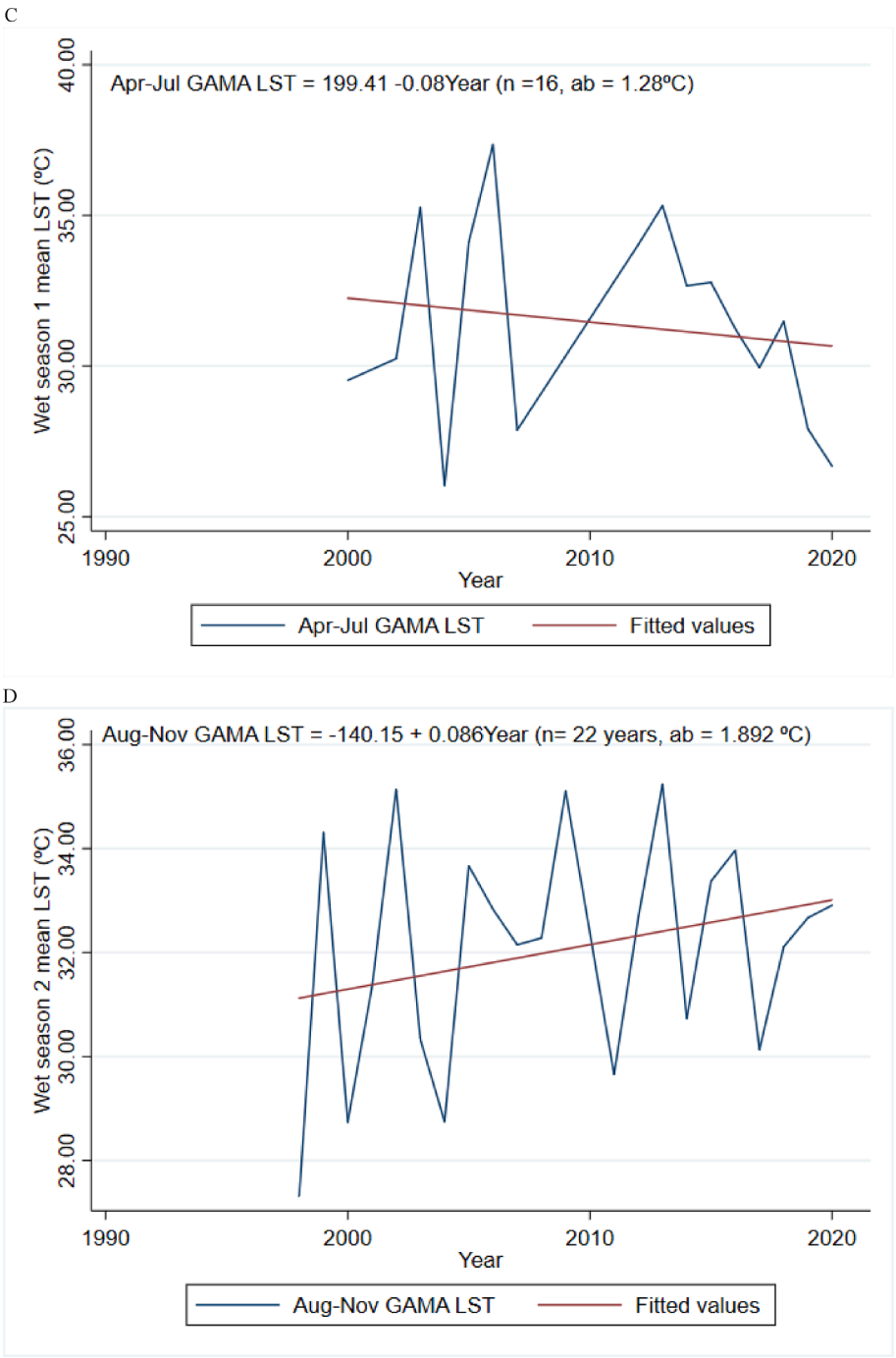

Fig. 4. (*continued*).

3.2. Economic implications for exchanging greens for heated surfaces

The LST was categorized according to the income status of each community (Fig. 10). The one-way ANOVA test revealed no statistically significant differences (see appendix 2.2 supplementary file 2.0 attached) in the minimum, maximum and mean LST across income status of the observed communities. This implies that the mean LST for the High ($\mu = 27.1 \pm 0.8$), Middle ($\mu = 26.7 \pm 1.2$) and Low ($\mu = 27.1 \pm 1.0$) income communities, is random (ANOVA $F^{cal} = 3.13$, p-value = 0.045, df = 2). The same applies to the minimum and maximum community LST. This means that there is no significant difference in the spatial pattern of LST between high, middle and low-income neighbourhoods.

3.3. Perceived health implications of exchanging greens for heated surfaces

3.3.1. Factors contributing to community heat exposure

The perceived factors contributing to the LST heat exposure risk in the communities are mainly the presence of impervious surfaces, the probability of being exposed to extreme heat exposure and the hours of extreme heat exposure during the day and night.

shows that a large proportion (73.0%, n = 65) of the respondents either agree (38.2% n = 34) or “strongly agree” (34.8%, n = 31) that impervious surfaces contribute to rising LST. About 18.0% (n = 16) were, however, indifferent while 3.4% (n = 3) and 5.6% (n = 5) were either “highly disagree” or “disagree” respectively. The results in

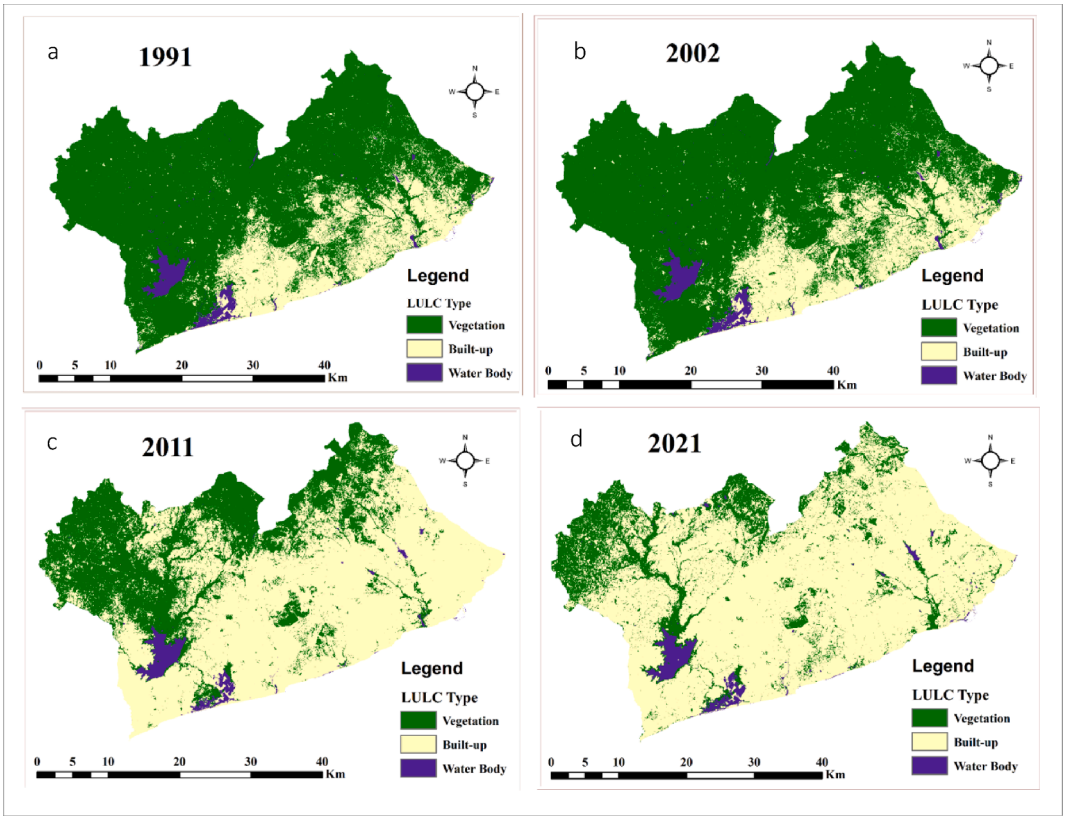

Fig. 5. Spatiotemporal pattern of land use land cover change in GAMA as of (a) 1991, (b) 2002, (c) 2011 and (d) 2021.

Table 4
Accuracy assessments of GAMA LULC classifications.

Accuracy	LULC Type	1991	2002	2011	2021
User's accuracy (%)	Vegetation	99.8	96.0	97.8	95.0
	Built-up	91.4	89.7	92.2	96.2
	Water Body	78.6	85.7	91.7	92.3
Producer's accuracy (%)	Vegetation	97.1	96.5	88.6	85.0
	Built-up	99.1	87.4	98.7	99.0
	Water Body	91.7	92.3	73.3	92.3
Overall accuracy (%)		**97.4**	**94.3**	**94.2**	**95.8**
Kappa Coefficient		**0.93**	**0.85**	**0.88**	**0.88**

Fig. 11b indicate that increase in the number of concrete buildings (86.5%, n = 77), concrete floors (66.3%, n = 59), tiled floors (52.8%, n = 47), tarred roads (51.7%, n = 46) and concrete pavements (49.4%, n = 44) are the common impervious surfaces in the observed communities.

3.3.2. *The extent of impervious surfacing in GAMA communities*

As shown in Fig. 12, a large proportion (66.9%, n = 69) of the participants indicated they were either "exposed" (41.7%, n = 43) or "highly exposed" (25.8%, n = 26) to extreme heat conditions where they spent most of the time. Only 28.2% (n = 29) were indifferent while 4.9% (5) said they were "highly unexposed".

3.3.3. *Residents perceived health risk of exposure to high LST*

Residents of the study communities recount their perceived exposed health risks due to high LST in their community. As shown in Fig. 13a, heavy sweating that causes discomfort (69.9%, n = 72) was expressed as the dominant perceived health risk of extreme heat, followed by headache (49.5%, n = 51), dehydration (48.5%, n = 50) and thirst (48.5%, n = 50). Informants indicated that their choices of answers were based on personal experience and perception (56.3% n = 58), medical advice, (21.4%, n = 22), lab diagnosis (7.8%, n = 8) and other sources such as friends and news. As shown in Fig. 13b, there was no statistically significant association of these health risks with the observed LST quintiles (Pearson chi-square = 49.2767 Pr = 0.837).

3.3.4. *Common adaptation strategies to health risks of rising LST*

Use of air conditioning devices (32.0%, n = 33), electric fans (31.1%, n = 32), opening of doors and windows and folding of curtains for more ventilation (25.2%, n = 26) are the common domestic adaptation strategies at home. Other adaptation strategies to rising LST (11.7%, n = 12) intimated by the respondents include taking a freshwater bath, using shade/shade trees, partially undressed, wearing light clothes, drinking more water, laying on a cold cement floor and staying indoors to minimize the health risk of high LST.

4. Discussion

4.1. *The extent of rising land surface temperature*

The results indicate that people living in the GAMA believe there are changes in the climate with rising LST in their communities, which impacts health and community economic status. The impact of Climate Change (CC) was confirmed by the LST analysis, which revealed that the highest maximum LST (49.0 °C) in 2021 and the lowest maximum (30.0 °C) in 1991 occurred at an increasing rate of 0.63°C per year. The mean LST rise (6.0°C) from 27.0°C to 33.0°C over the 30 years at a rate of 0.20°C per annum was based on four Landsat datasets. These findings are consistent with some previous global studies (Easterling et al., 1997; Nangombe et al., 2019; Roy et al., 2020; Saha et al., 2021). Roy et al. (2020) reported an increase of 5.6°C in the mean LST (20.2°C to 25.8°C) between 1990 and 2018 in the Chatogram Metropolitan Area in Bangladesh. Nangombe et al. (2019) indicated a similar rise of LST in South and West Africa while Easterling et al. (1997) anticipated a 3-5°C

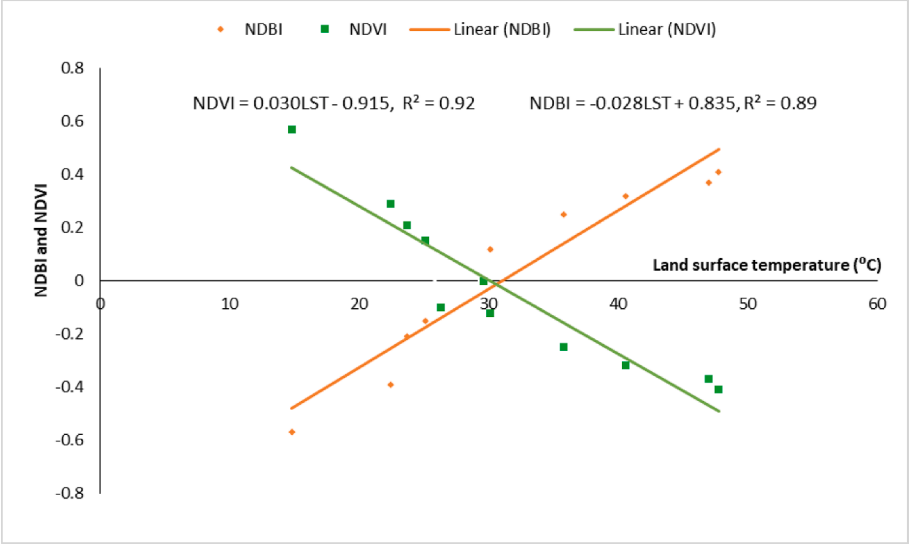

Fig. 6. The relationship between land surface temperature (LST), built-up (NDBI) and vegetation (NDVI) indexes of GAMA.

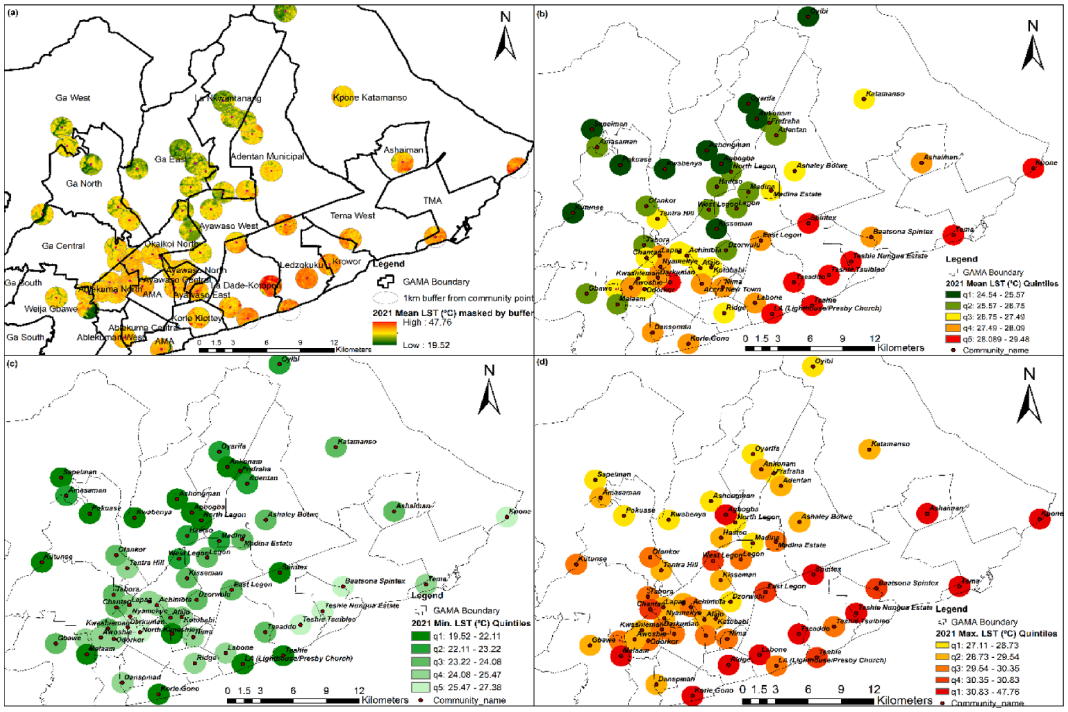

Fig. 7. Spatial variability (a), maximum (b), minimum (c) and mean (d) land surface temperature of GAMA communities as of 2021.

Table 5
Descriptive statistics of the long-term community-level annual LST quintile.

Community	LST quintile (LSTq)	Period	Years	Mean (°C)	Std. Dev. (°C)	Min (°C)	Max (°C)
Tema	q5 (≤100th %)	1991, 1998–2021	25	35.0	2.4	26.1	37.7
Dansoman	q4 (≤80th %)	1991, 1998–2021	25	34.8	1.4	31.9	37.6
Ridge	q3 (≤60th %)	1991, 1999–2021	24	33.6	1.7	30.3	36.8
Legon	q2 (≤40th %)	1991, 1999–2021	24	32.8	2.3	25.4	35.5
Kisseman	q1 (≤ 20th %)	1991, 1999–2021	24	31.0	2.3	23.3	34.8
Missing data in 1992–1998							

rise in airT of tropical regions in Africa by the end of the 21st century. This pattern of rising LST is consistent with other authors (Saha et al., 2021), who estimated a 1.5 to 3.5°C increase over the last 30 years for English Bazaar Urban Agglomeration. The increase in GAMA's mean LST of 4.0°C from 2002 to 2011 is far higher than the projected global estimate of 0.99°C in the recent AR6 report by IPCC (2021). However, the

observation for 2011–2021 in GAMA falls short by 2.0°C when compared to the IPCC's estimate of 1.09°C for 2011–2020. The 6.0°C was based on only four Landsat data sets and thus watered down when cross-validated using more data in using the GEE approach. The rise turned out to be 0.8°C at an annual rate of 0.03 °C in 25 years. Nonetheless, this 0.8°C mean LST rise has important livability implications for GAMA. The IPCC's alarm that many urban areas would experience more than a 1.5–2.0°C rise in temperature by 2050. This therefore should be of concern to the GAMA communities, especially in LSTq5 communities like Tema to plan for a climate-resilient city. This is because it would only take massive and immediate effort to avert the projected 1.5–2.0°C increase in temperature (IPCC, 2021) for sustainable living.

4.2. The extent of increasing built-up, decreasing vegetation and water body

We found that the built environment in GAMA grew by 258.7% (849.6 km^2) at an annual rate of 8.6% in the 30 years. On the contrary, vegetation cover experienced a decline of 74.6% (846.3 km^2) at 2.5% per annum. The water bodies also decreased by 3.3 km^2. All these findings are consistent with Owusu (2018) and Addae and Oppelt, (2019), who reported that the built environment in GAMA grew by 277% in 24 years while the forest cover decreased alongside the waterbody in 25 years (1991 and 2015). Several socioeconomic factors have contributed to the rapid expansion of the built environment (Doe et al., 2018; Owusu, 2018). Apart from human population growth, GAMA witnessed significant private capital investment in the housing sector through real estate development from both local and foreign investors (Addae and Oppelt, 2019; Mantey et al., 2014). These investments were aimed at meeting the housing needs of expatriates and expected diaspora returnees living abroad. This real estate development is conspicuous in the Accra Metropolitan Area (AMA), Tema, Korley Klotey, Tseaddo among other MMDAs (Addae and Oppelt, 2019).

In contrast to high-income countries like Germany, UK or USA, expansion of the built environment in GAMA is rarely shaped by economic development and spatial planning. While increased productivity and industrialization are notable attributes of urbanization in the Western world, the experience in Africa is often not the same (Songsore, 2020; Songsore and McGranahan, 2012). The expansion of the built environment is also largely due to human population growth and rural–urban migrants trying to settle in the city and its outskirts, in low-cost or underdeveloped green spaces. Songsore (2020) noted this as demographic urbanization rather than economic urbanization. Poverty-driven rural–urban migration is often characterized in communities by crowding of houses, poor environmental sanitation management and heat effects (Songsore et al., 2006).

A major consequence of unregulated (unplanned) spatial expansion of the built environment is the loss of vegetation cover. This includes the loss of green spaces which are useful for controlling air pollution, providing walkable, recreational and playable spaces for adults and children (Adjei-Boadi et al., 2022). A changing dynamic is demonstrated by the findings from LULCC influencing UHI. To make cities nature-friendly, livable and resilient, there must be considerable urban revitalization through urban green development, open space and landscape management strategies (Dissanayake et al., 2019). As proposed by Ojeh et al. (2016) it is necessary to design climate-smart cities with nature-friendly urban planning systems and this may include city decongestion, open space management and decentralised economic activities that are separate from the city centre (Mantey et al., 2014; Puplampu and Boafo, 2021). Spatial development planning needs to be employed to control the growth of built-ups with green open spaces (Ningrum, 2018). Also, to improve the thermal environment and mitigate UHI, there is the need for the use of lower absorptive material, higher reflective and larger thermal conductivity of buildings (Ningrum, 2018), restoration and protection of wetlands (Völker et al., 2013) and introduction of cool roof and green roof (Malley et al., 2015; Zhang et al., 2017) as well as promoting urban forestry within GAMA. As iterated by Jenerette et al. (2016), the cooling of hotter neighbourhood is more effective with vegetation. Planting of shade trees supports the arguments of Chen et al. (2022) and Li (2020), who indicated varied cooling approaches for mitigating temperature rise and urban microclimate. These cooling approaches involve green, blue and grey infrastructures for cooling the microclimate of different urban facilities across various urban land use types.

The green infrastructure is strategically a network of high-quality natural and semi-natural areas with other environmental features,

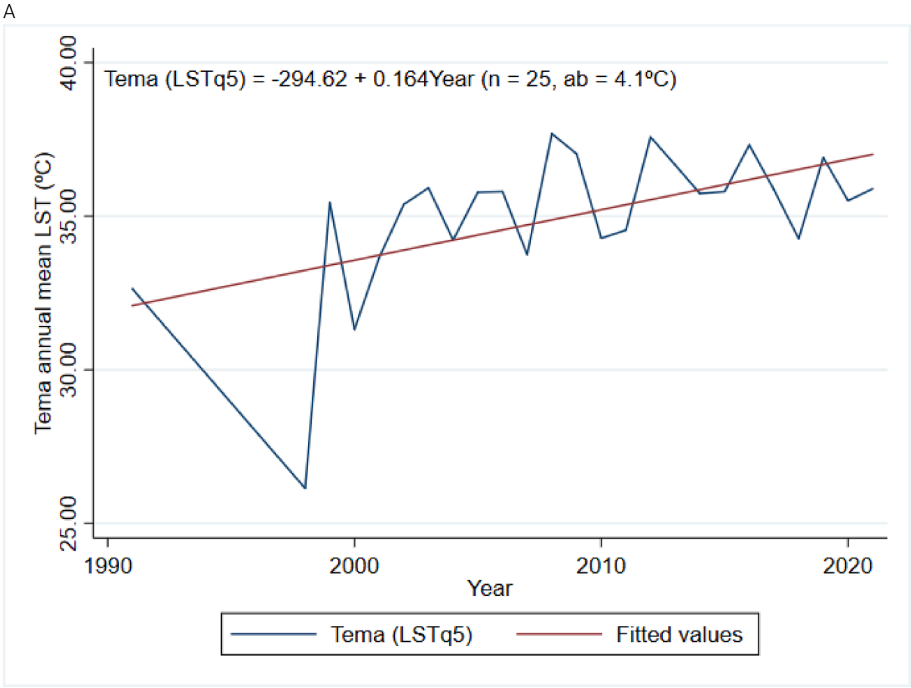

Fig. 8. Time Trends of annual LST in Tema (a), Dansoman (b), Ridge (c), Legon (d) and Dansoman (e), (n = number of years; ab = absolute change ±).

B

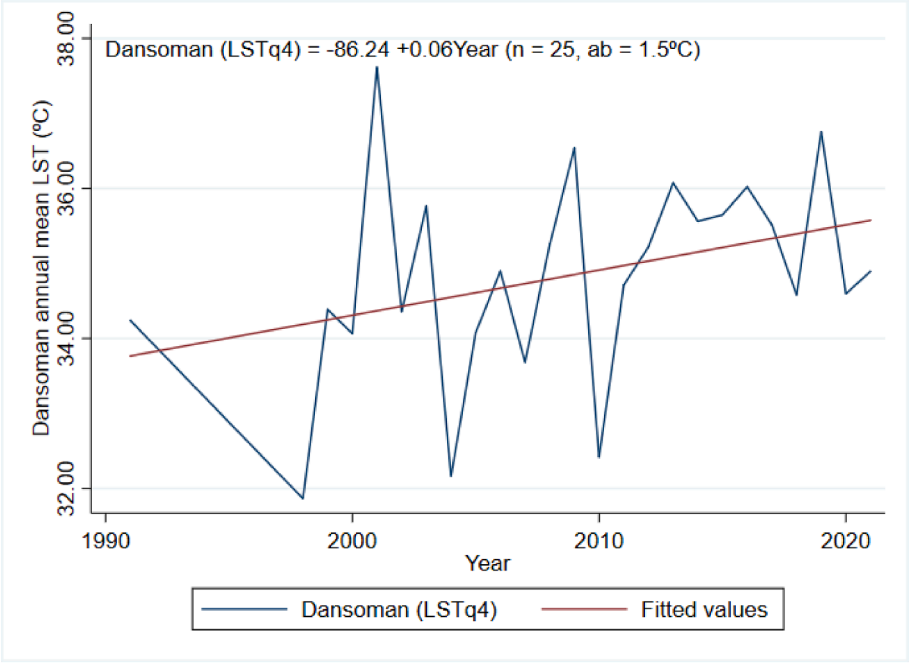

C

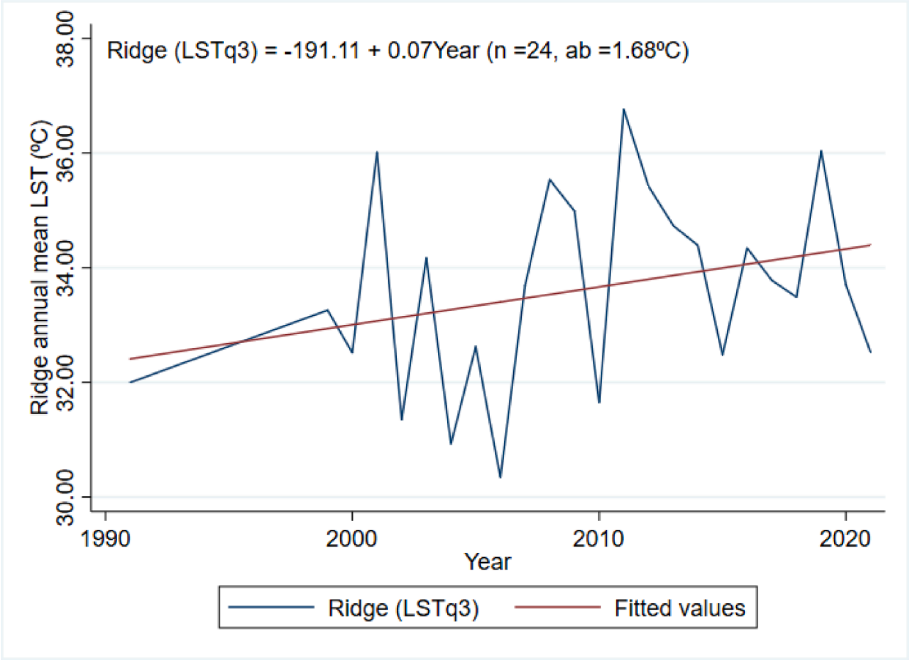

Fig. 8. (*continued*).

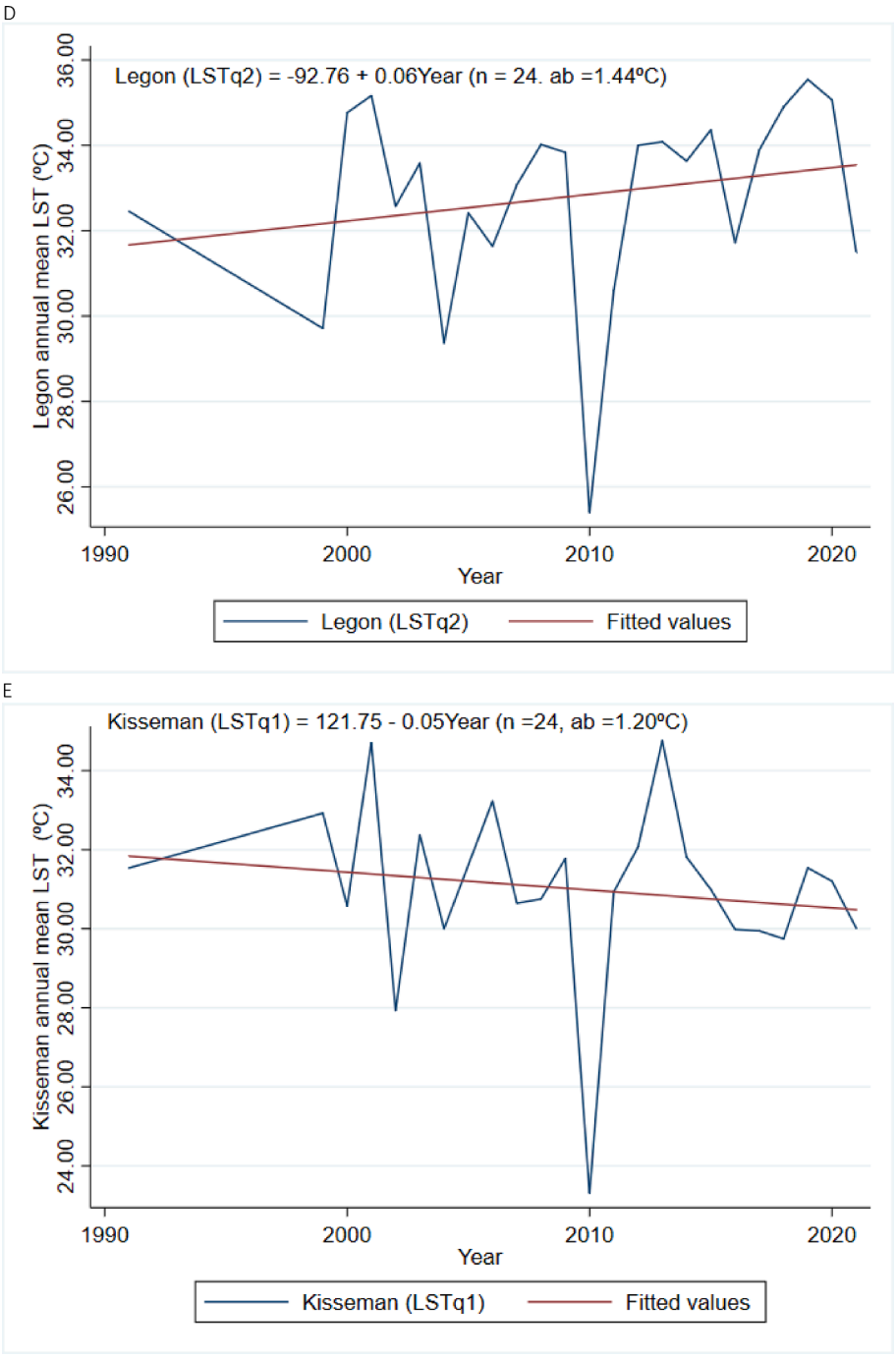

Fig. 8. (*continued*).

designed and managed to provide a variety of ecosystem services. The grey infrastructure is man-made features such as pipes, ditches, swales, culverts, and retention ponds that provide the same services (Li et al., 2020). The blue infrastructure relates to urban water systems such as ponds, lakes, streams, rivers and stormwater management systems to provide ecosystem services. Li et al. (2020), proposed that while each of the "colour" strategies is good individually, an integrated green, blue and grey infrastructure is also key. For instance, the combination of trees and pavilions has a much stronger cooling effect than either trees or pavilions alone (Xu et al., 2017). Li et al (2020) also suggested that treated wastewater could be suitable for parks, gardens and squares while green infrastructure should be applied to residential areas. The integrated strategy includes high raising buildings to reduce impervious surfaces within the built environment. Digital agriculture as suggested by Jiang et al. (2022) is another way to improve urban microclimate. According to Jiang et al. (2022), use of information technologies like artificial intelligence, robotics, phones, internet and e-commerce in digital agriculture can improve the efficiencies of agricultural activities to reduce greenhouse gas emissions.

4.3. The point of inflexion in the inverse relationship of LST, vegetation and built-up

Another finding of the study is the 30.0ºC LST point of inflexion (tipping point) that pivots the inverse relationship between vegetation loss and rising built-up environment, spurring UHIs in GAMA. This 30ºC

is the tipping point beyond which the built-up area overtakes the vegetation area in size and vice-versa in GAMA. This inverse relationship is consistent with many authors (Fu and Weng, 2016; Ning et al., 2018; Tuffour-Mills et al., 2020; Zhang et al., 2009). For instance, Tuffour-Mills et al. (2020), reported a similar relationship in Ghana. This finding implies that at a mean LST of 30°C there is a zero correlation between vegetation and built-up cover. Above 30°C, there is a negative correlation between vegetation and built-up LULCC. Many authors including Ning et al. (2018) noted this point of inflexion at different thresholds of LST and LULCC in their studies. Essentially, this finding provides a statistical guide for checking the imbalance (inequality) of vegetation cover and built-up area cover in GAMA.

The drivers of vegetation loss and rising LST can be associated with the expansionary trend of built-up, particularly impervious surfaces as depicted by the inverse correlation explained below and illustrated in land surface quintiles (LSTq) of Fig. 7 and Fig. 14. This observed phenomenon confirmed the report of Ahmed (2018), Pelta and Chudnovsky, (2017) and Puplampu and Boafo (2021). The UHI effect is experienced in most populated and high-density built-up environments and rarely in vegetative zones in Egypt, Tel-Aviv, Accra Metropolitan Areas (Ahmed, 2018; Pelta and Chudnovsky, 2017; Puplampu and Boafo, 2021). This finding also buttresses the point of Sun et. al, (2012), Songsore and McGranahan (2012) and Xu et al. (2021), that an increasingly impervious surface changes the properties of the ground surface and directly impacts the LST of urban ecology. According to Imhoff et. al, (2010) and Sun et. al, (2012) urban LST increases with an increasing density of built-up areas and decreases with vegetation cover growth.

4.4. *Spatial differences in decreasing and increasing temperature at the community level*

Characterizing the observed communities into five LST quintiles (Fig. 7&14), it was found that communities that harbour the central business district and manufacturing industries belong to the highest (fifth) LSTq (28.5°C ± 0.4). The highest LSTq5 communities had more buildings, tarred, paved or tiled surfaces and few vegetation areas than other communities. This corroborates Fu and Weng (2016) and Meyers et al. (2020) that built infrastructure generates higher heat-holding capacity during the day and releases it gradually at night and this causes the UHIs. The findings also agree with Das and Das (2022), who indicated higher LST within built-up environments.

The fourth quintile (LSTq4) communities are known for their high-density human populations, transport activities and housing facilities. They also had some bare land (football parks) and little vegetation. Although some hot surface temperatures were found in places that contained extensive bare land and sparse vegetation, Meyers et al. (2020) explained that the sparse vegetation and bare land cover cool down more quickly at night. They are also relatively cooler during wet periods than in the built environment (Meyers et al., 2020). The second LSTq2 and first LSTq1 communities are known for having fewer built

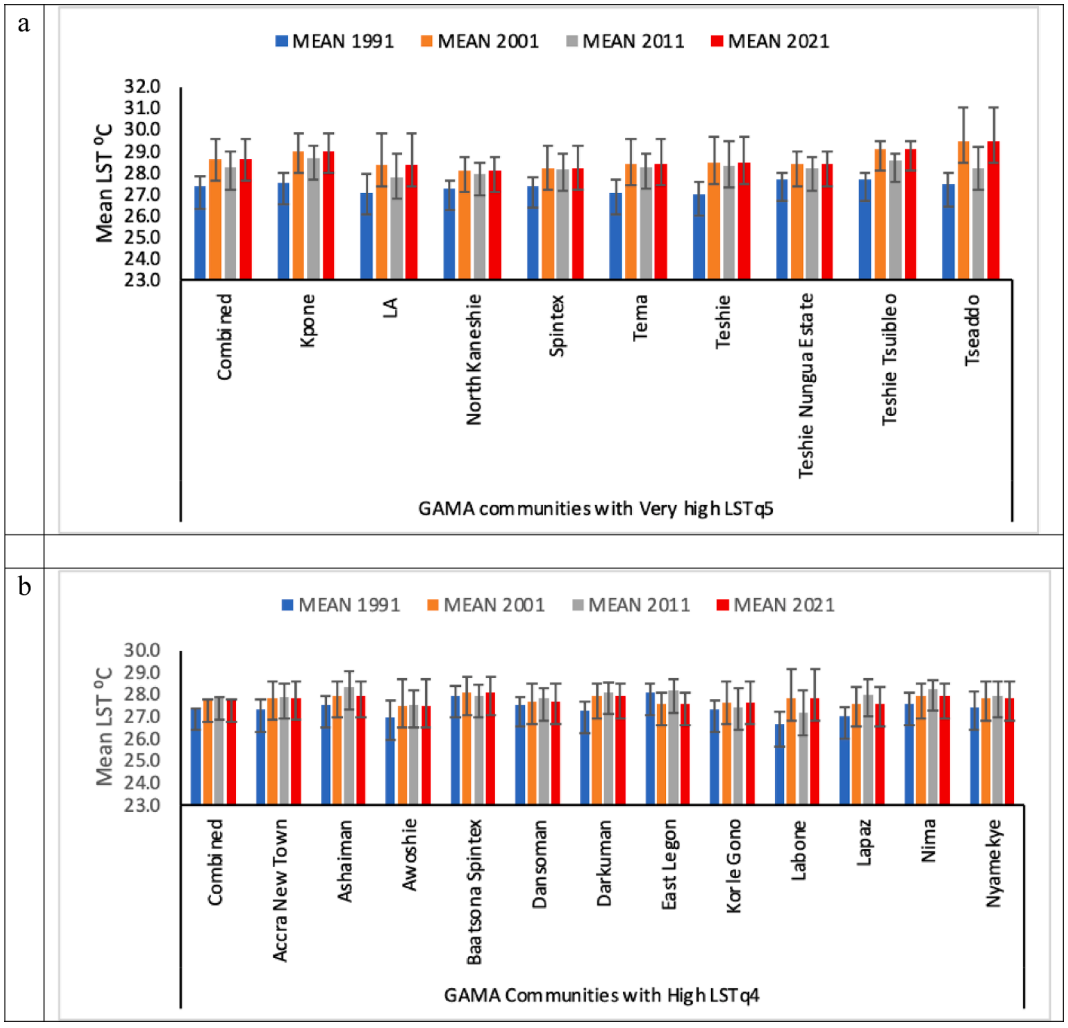

Fig. 9. Trends of GAMA community-level land surface temperature (LST) from 1991 to 2021 in (a) Very high, (b) High, (c) Moderate, (d) Low and (e) Very low LST quintiles.

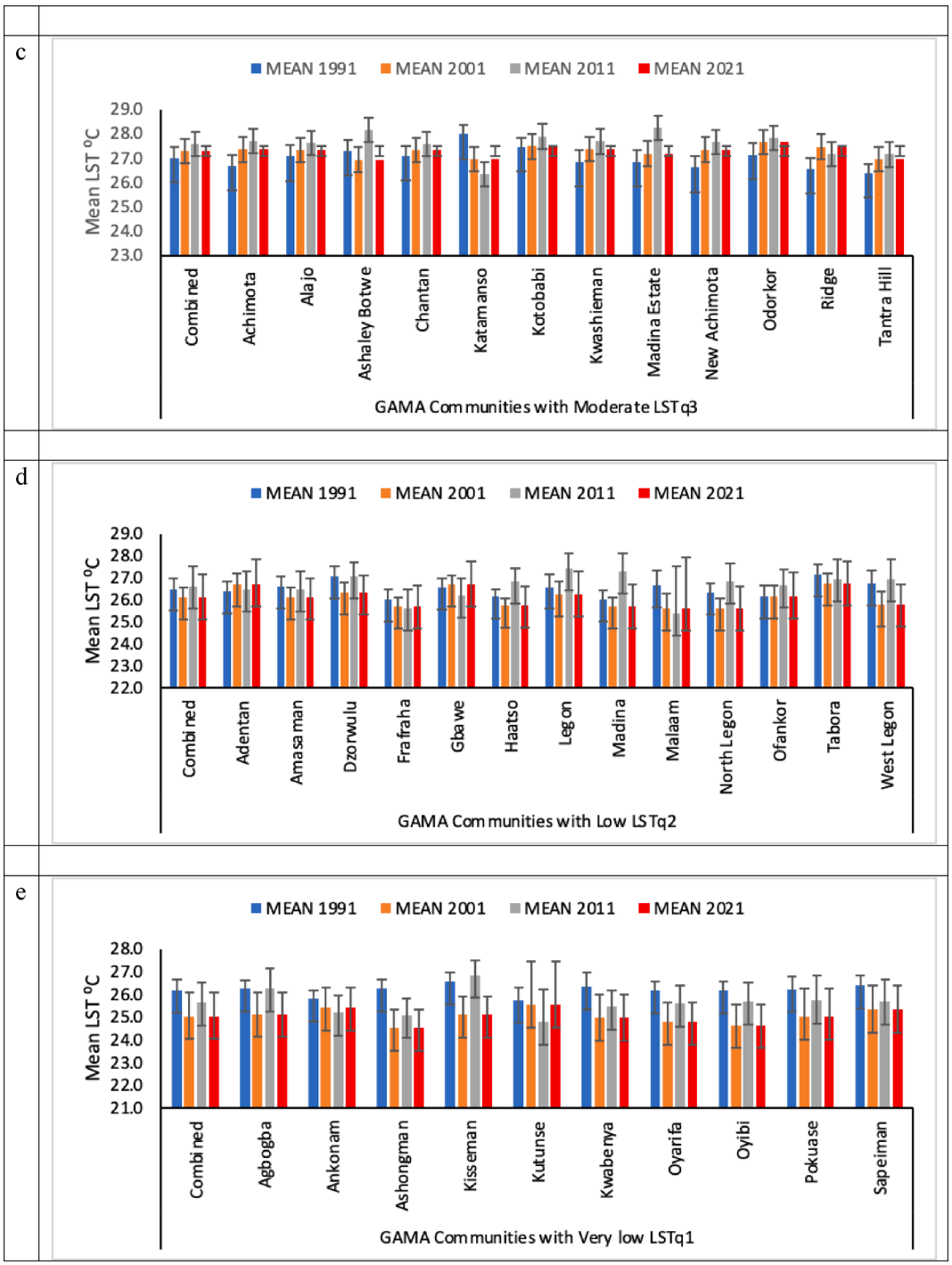

Fig. 9. (*continued*).

environments, bare lands and extensive vegetative cover encompassing the Legon West and the Achimota Forest Reserve near Kisseman.

Source: Google Earth, 2022; Assessed on 20/01/2022; 13:14.

Furthermore, the trends of communities LST soared in the very high, high and moderate LSTq communities but decreased in the low and very low LSTq communities. The rising LST in the former may be attributed to the building of more impervious surfaces, corroborating (Chen et al., 2022; Quan et al., 2022). On the contrary, the trend of decreasing LST in the low and very low LSTq may be due to low-density residential development, frequency of rainfall due to their proximity to highlands and land litigation which has delayed urban development in those areas as portrayed Zhao et al., (2021). In other words, the lower LSTq communities had a lesser anthropogenic impact on the natural land surface than the higher LSTq communities and vice versa.

4.5. *Land surface temperature implications for economic status and health risks*

The relation between the community LST and income status of GAMA communities was found to be statistically insignificant. In China, the expansion of heated surfaces, radiated from high-income urban core areas to replace vegetative cool areas outside the core business districts of Hangzhou (Lin et al., 2018). Therefore, the insignificance of the community LST and income-status nexus in GAMA is incongruent with

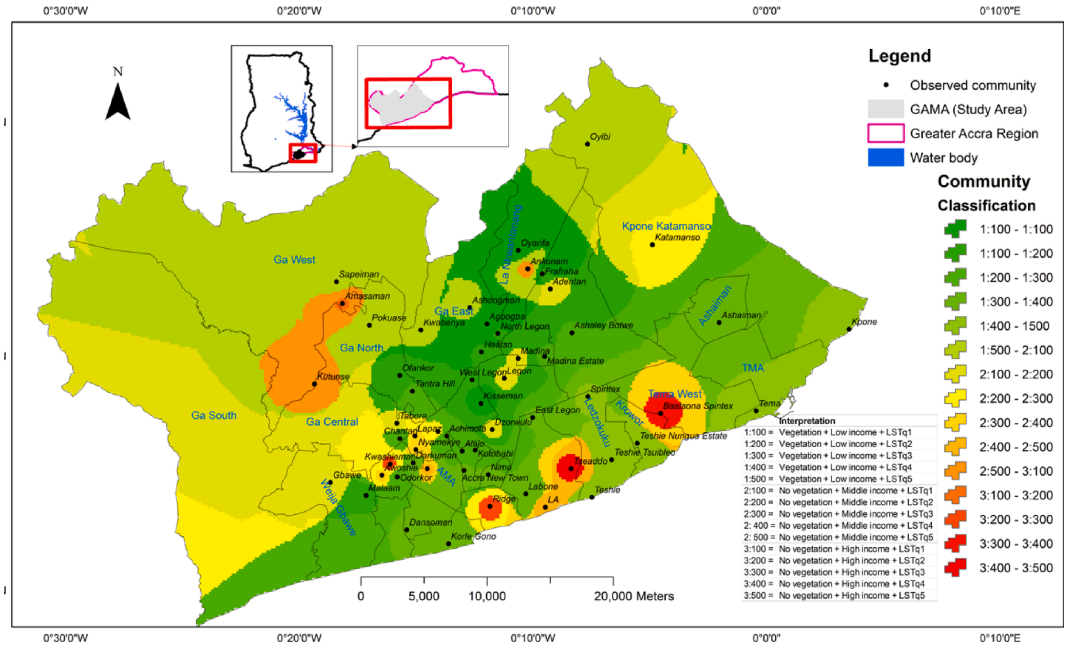

Fig. 10. Spatial correlation of community income status, vegetation and LST quintiles in GAMA as of 2021.

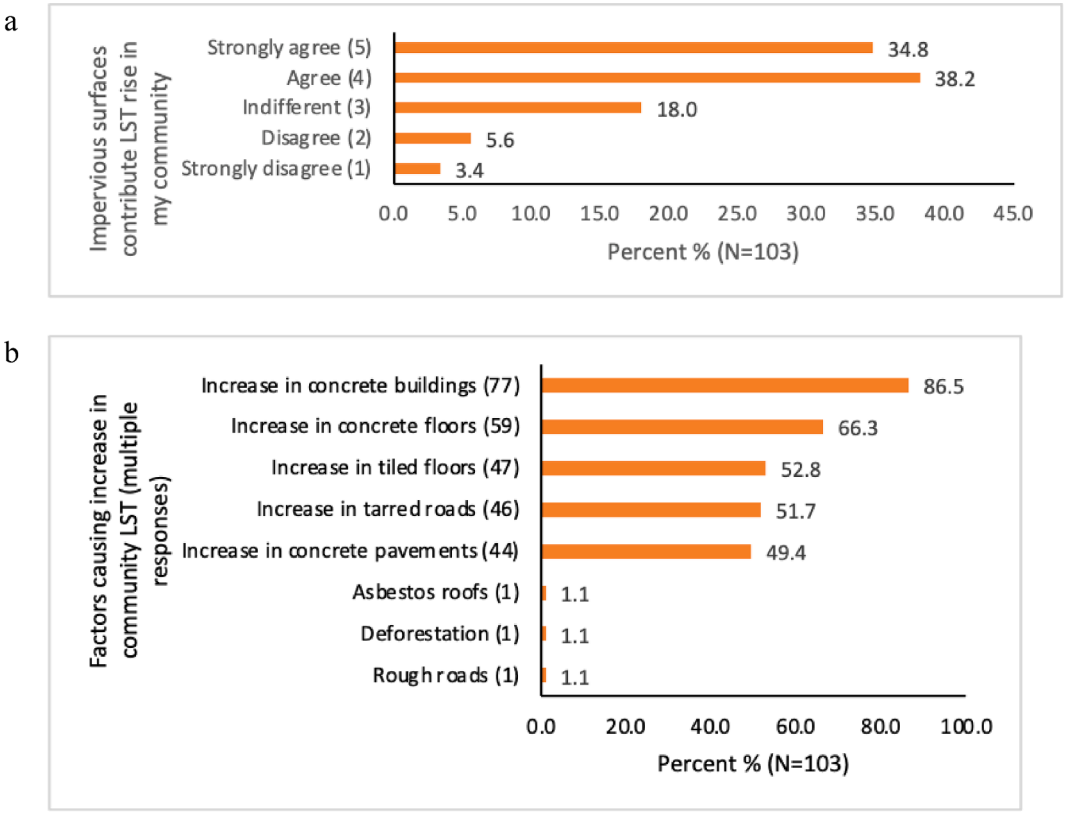

Fig. 11. (a) Contribution of impervious surfaces to LST and (b) common impervious surfaces in the observed communities.

many others (Lin et al., 2018; Sun et al., 2021). It contradicts Sun et al., (2021) who reported that the status of socioeconomic activities drives vegetative cover loss and UHIs in Hangzhou. Hangzhou harbours high-technological industrial activities and impervious surfaces. The insignificance of the current observation might be due to less industrial activities in most of the observed high-income communities like Ridge in the current study.

However, the relation between the community LST and health risk in GAMA was statistically significant. This finding corroborates Jenerette et al. (2016) who reported that urban LST driven by land cover features impacts residential heat-related health risks, in Phoenix (Arizona) USA. In GAMA. The finding is also consistent with Das and Das (2016) who reported that outdoor LST thermal conform within built-up areas was more uncomfortable than other land cover types. The perceived common health risks of high LST include heavy sweating, headache, dehydration, intense thirst and skin rashes. These findings affirm WHO

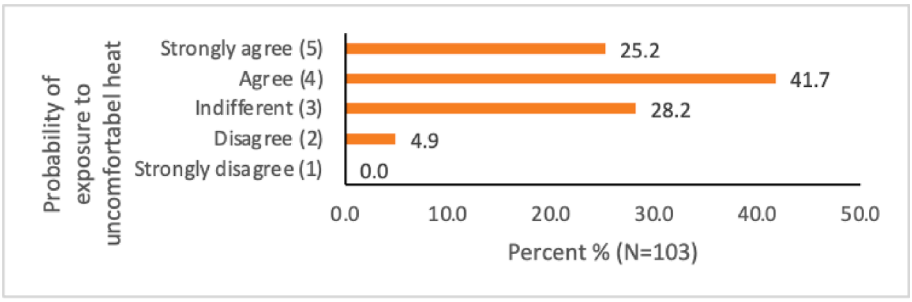

Fig. 12. Perceived probability (Likert scale of 1 to 5) of exposure to heat conditions by participants.

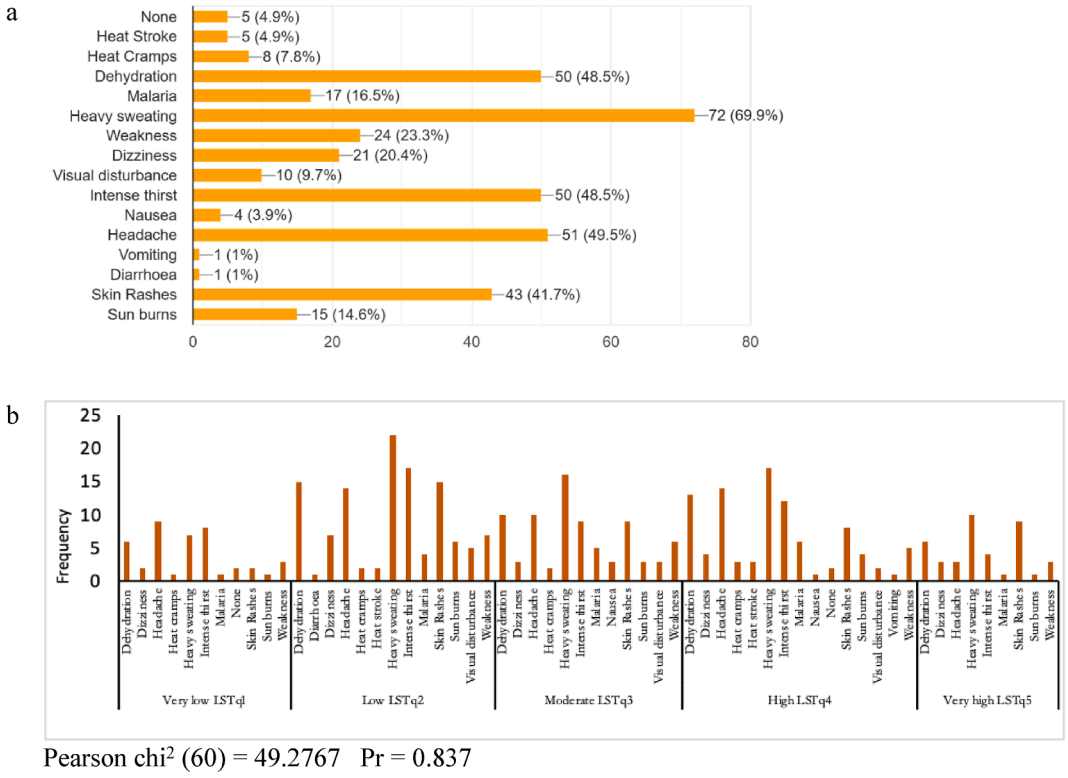

Fig. 13. (a) Perception of common health risk (a) associated with heat exposure and (b community-level land surface temperature quintile.

(2013), Mantey et al. (2014) and Krehbiel et al. (2016). According to WHO (2013) and Jenerette et al., (2016), there are many of these heat related-health effects of rising LST to be avoided. Elsewhere, high LST exacerbates city heat and air pollution by causing smog. Smog is a hazardous pollutant that makes it harder to breathe leading to asthma attacks most frequently among children (WHO, 2013). Therefore, strengthening key health systems and improving the management of the health risks of UHI would be required in GAMA. Some of the health adaptation strategies of the urban community dwellers in GAMA corroborate Mantey et al. (2014) and Puplampu et al. (2021). The observed high LST adaptation strategies encompass planting shade trees, use of air conditioning (AC) and electric fans, opening doors and windows and folding curtains for more ventilation. Some of these adaptation strategies like ACs may create environmental liabilities. Opening doors may increase mosquitoes in rooms, whiles the use of air conditioners increases household energy bills. According to Kayaga et al. (2021), extreme heat events create high demand for water and electricity and this demand exceeds supply, leading to shortages and severe pressure on water and energy resources in Ghana. Other adaptation strategies like taking a freshwater bath, using shade/shade trees, partially undressed, wearing light clothes, drinking more water, laying on a cold cement floor and leaving the home are also common. Therefore, green, blue and grey spatial planning of city cooling systems remains crucial for sustainable city growth in the face of LULC and LST changes and health risks (Jenerette et al., 2016; Chen et al., 2022).

4.6. *Data limitations*

Data used for this study included; (1) the Landsat satellite images downloaded from the USGS website at a spatial resolution of 30 m and in the month of December which is the dry season and therefore measuring peak period temperature and not the average for the year. Again, using a single scene image may not reflect the annual temperature, however, this was necessitated by the lack of cloud-free data. In making up for the shortfall, we used google earth engine archive data to provide time series on temperature, which to a large extent reflects annual temperature trends. It's equally true that the google earth engine may not have provided the entire scene at a time, it helps in generating the annual average temperature. In this study, using google earth engine provided 341 Landsat images in estimating the annual for the study period of 25 years.

(2) The primary data used in assessing local perception was based on

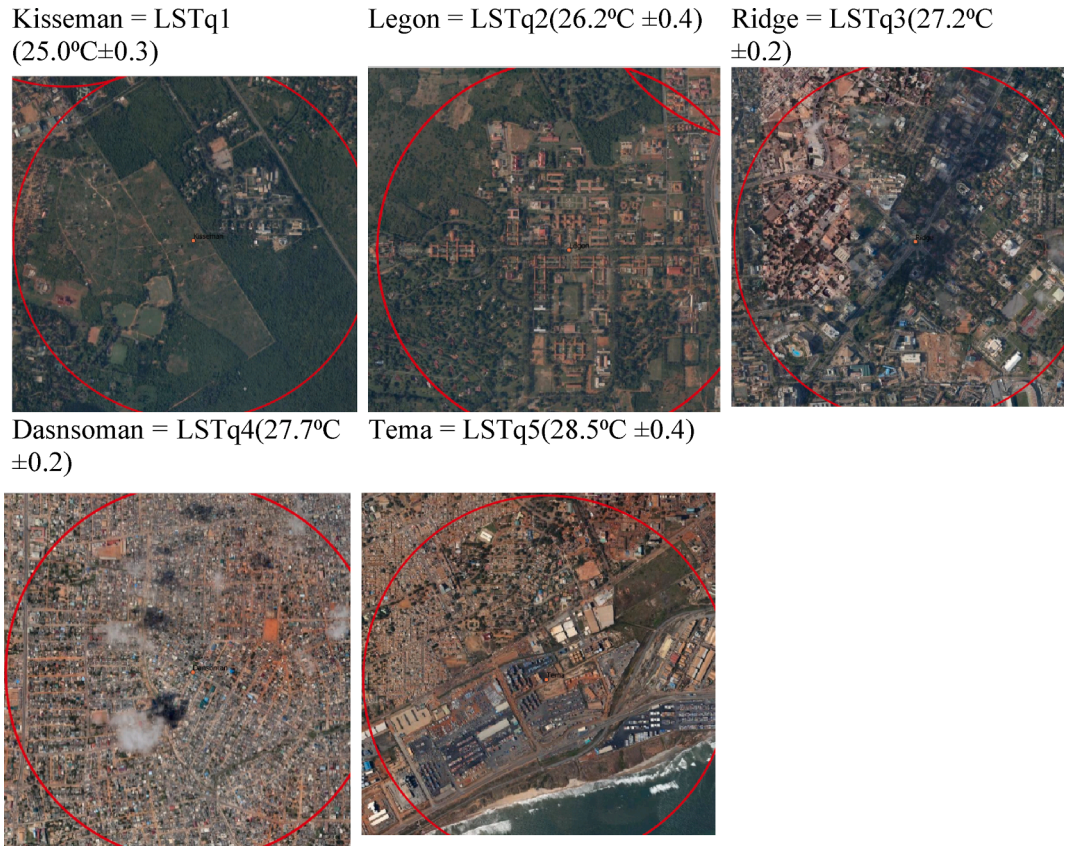

Fig. 14. Rising land surface temperature quintiles.

a semi-structured questionnaire we designed using google forms and administered online through social media platforms to conduct a cross-sectional assessment of socioeconomic and health risks of urban LST in GAMA. The biggest limitation is the fact that the study has no control over the respondents' selection. Such a method of data collection often favors the educated population and their understanding of the questions. However, we find the data useful given that 103 respondents from 56 communities actually responded to the survey. Perhaps the 103, may constitute a small response, but the relevance is the point that we did not make inferences from the study, rather it is an opinion study and the respondents were fairly distributed across the entire study area.

We concluded that the study data may have some limitations, it useful and the findings were equally relevant as they concur with many other recent studies including Puplampu, and Boafo, 2021; and Owusu, 2018.

5. Conclusions

In conclusion, the current study has adduced new evidence that advances the frontiers of knowledge concerning the relationship of LST, NDVI, NBVI and their health risks implications to urban community dwellers in GAMA. The built environment grew by 258.7% (849.6 km^2) at an annual rate of 8.6% while the vegetation declined by 74.6% (846.3 km^2) at 2.5% per annum. The mean LST of GAMA rose by 0.8ºC in 30 years at 0.03ºC per annum. A mean LST of 30ºC corresponds to the tipping point in the inverse relationship between vegetation and the built environment. The trends of community LST increased in the very high, high and moderate LST quintile communities, but the LST decreased in the low and very low LST quintile communities. The income status of communities did not reflect their LST quintiles. While the general LST of GAMA increased and study participants express discomfort with heated rooms and outdoor temperatures had health risks implications. The common health risks of extreme heat/urban heat islands include heavy sweating that causes discomfort, headaches, dehydration and intense thirst. The differences in community LST and income status were not statistically significant. This implies that relying on community-level or local microclimate estimates to inform LST policy can misguide decisions and the urgency of taking climate action. The policy implication of this study points to a need for prioritizing efforts to curb trade-offs of green spaces for heated surfaces and its health and climate action implications. It calls for urban forestry and sustainable climate-resilient city development of GAMA communities. These include building multi-purpose green cooling housing, roads, health and industrial infrastructure.

Declaration of Competing Interest

The authors declare that they have no known competing financial interests or personal relationships that could have appeared to influence the work reported in this paper.

Appendix A. Supplementary material

Supplementary data to this article can be found online at https://doi.org/10.1016/j.ejrs.2023.09.004.

References

Acheampong, R.A., 2019. Spatial planning and the urban informal economy. Spatial Planning Ghana. https://doi.org/10.1007/978-3-030-02011-8.

Addae, B., Oppelt, N., 2019. Land-use/land-cover change analysis and urban growth modelling in the Greater Accra Metropolitan Area (GAMA). Ghana. Urban Sci. 3, 26. https://doi.org/10.3390/urbansci3010026.

Adeyeri, O.E., Akinsanola, A.A., Ishola, K.A., 2017. Investigating surface urban heat island characteristics over Abuja, Nigeria: Relationship between land surface temperature and multiple vegetation indices. Remote Sens. Appl.: Soc. Environ. 7, 57–68. https://doi.org/10.1016/j.rsase.2017.06.005.

Adjei-Boadi, D., Agyei-Mensah, S., Adamkiewicz, G., Rodriguez, J.I., Gemmell, E., Ezzati, M., Baumgartner, J., Owusu, G., 2022. Neighbourhood, built environment and children's outdoor play spaces in urban Ghana: Review of policies and challenges. Landsc. Urban Plan. 218, 104288 https://doi.org/10.1016/j.landurbplan.2021.104288.

Afaq, Y., Manocha, A., 2021. Ecological Informatics Analysis on change detection techniques for remote sensing applications : a review. Ecol. Inform. 63, 101310 https://doi.org/10.1016/j.ecoinf.2021.101310.

Ahmed, S., 2018. Assessment of urban heat islands and impact of climate change on socioeconomic over Suez Governorate using remote sensing and GIS techniques. Egypt. J. Remote Sens. Sp. Sci. 21, 15–25. https://doi.org/10.1016/j.ejrs.2017.08.001.

Ampim, P.A.Y., Adiku, S.G.K., Sloan, J.J., 2015. Green roofs : A possible best management practice for enhancing the environmental quality of Ghanaian cities 9, 701–711. doi: 10.5897/AJEST2014.

Athukorala, D., Murayama, Y., 2020. Spatial variation of land use/cover composition and impact on surface urban heat island in a tropical sub-Saharan City of Accra Ghana. Sustain. 12 (19), 7953. https://doi.org/10.3390/SU12197953.

Avashia, V., Garg, A., Dholakia, H., 2021. Understanding temperature related health risk in context of urban land use changes. Landsc. Urban Plan. 212, 104107. https://doi.org/10.1016/j.landurbplan.2021.104107.

Chen, S., Haase, D., Qureshi, S., Firozjaei, M.K., 2022. Integrated land use and urban function impacts on land surface temperature: implications on urban heat mitigation in berlin with eight-type spaces. Sustain. Cities Soc. 83, 103944.

Codjoe, S.N.A., Gough, K.V., Wilby, R.L., Kasei, R., Yankson, P.W.K., Amankwaa, E.F., Abarike, M.A., Atiglo, D.Y., Kayaga, S., Mensah, P., Nabilse, C.K., Griffiths, P.L., 2020. Impact of extreme weather conditions on healthcare provision in urban Ghana. Soc. Sci. Med. 258, 113072 https://doi.org/10.1016/j.socscimed.2020.113072.

Das, M., Das, A., 2020. Exploring the pattern of outdoor thermal comfort (OTC) in a tropical planning region of eastern India during summer. Urban Clim. 34 (August), 100708 https://doi.org/10.1016/j.uclim.2020.100708.

DESA-UN DESA-UN, 2018. World Urbanization Prospects: The 2018 Revision, Demographic Research. New York.

Dissanayake, D., Morimoto, T., Murayama, Y., Ranagalage, M., Handayani, H.H., 2019. Impact of urban surface characteristics and socio-economic variables on the spatial variation of land surface temperature in Lagos City, Nigeria. Sustain. 11 (1), 25.

Doe, E.K., Aikins, B.E., Njomaba, E., Owusu, A.B., 2018. Land use land cover change within Kakum Conservation Area in the Assin South District from 1991–2015. West African J. Appl, Ecol.

Easterling, D.R., Horton, B., Jones, P.D., Peterson, T.C., Karl, T.R., Parker, D.E., Salinger, M.J., Razuvayev, V., Plummer, N., Jamason, P., Folland, C.K., 1997. Maximum and minimum temperature trends for the globe. Science 277 (5324), 364–367.

Ermida, S.L., Soares, P., Mantas, V., Göttsche, F., Trigo, I.F., 2020. Google earth engine open-source code for land surface temperature estimation from the landsat series. Remote Sens. 12, 1471. https://doi.org/10.3390/rs12091471.

Foody, G.M., 2020. Explaining the unsuitability of the kappa coefficient in the assessment and comparison of the accuracy of thematic maps obtained by image classification. Remote Sens. Environ. 239, 111630 https://doi.org/10.1016/j.rse.2019.111630.

Fu, P., Weng, Q., 2016. A time series analysis of urbanization induced land use and land cover change and its impact on land surface temperature with Landsat imagery. Remote Sens. Environ. 175, 205–214.

Ghana Statistical Service, 2021. Ghana 2021 Population and Housing Census, Population of Regions and Districts, Volume 3A. Accra, Ghana.

Gonzalez-Trevizo, M.E., Martinez-Torres, K.E., Armendariz-Lopez, J.F., Santamouris, M., Bojorquez-Morales, G., Luna-Leon, A., 2021. Research trends on environmental, energy and vulnerability impacts of Urban Heat Islands: an overview. Energ. Buildings 246, 111051. https://doi.org/10.1016/j.enbuild.2021.111051.

Guha, S., Govil, H., Gill, N., Dey, A., 2021. A long-term seasonal analysis on the relationship between LST and NDBI using Landsat data. Quat. Int. 575–576, 249–258. https://doi.org/10.1016/j.quaint.2020.06.041.

Halder, B., Bandyopadhyay, J., Banik, P., 2021. Monitoring the effect of urban development on urban heat island based on remote sensing and geo-spatial approach in Kolkata and adjacent areas, India. Sustain. Cities Soc. 74, 103186 https://doi.org/10.1016/j.scs.2021.103186.

Huang, C., Davis, L.S., Townshend, J.R.G., 2002. An assessment of support vector machines for land cover classification. Int. J. Remote Sens. 23, 725–749. https://doi.org/10.1080/01431160110040323.

Huang, S., Tang, L., Hupy, J.P., Wang, Y., Shao, G., 2021. A commentary review on the use of normalized difference vegetation index (NDVI) in the era of popular remote sensing. J. For. Res. 32, 1–6. https://doi.org/10.1007/s11676-020-01155-1.

Imhoff, M.L., Zhang, P., Wolfe, R.E., Bounoua, L., 2010. Remote sensing of the urban heat island effect across biomes in the continental USA. Remote Sens. Environ. 114, 504–513. https://doi.org/10.1016/j.rse.2009.10.008.

IPCC, 2021. Climate Change 2021: The Physical Science Basis. Contribution of Working Group I to the Sixth Assessment Report of the Intergovernmental Panel on Climate Change [Masson-Delmotte, V., P. Zhai, A. Pirani, S. L. Connors, C. Péan, S. Berger, N. Caud, Y. Chen,. Cambridge Univ. Press In Press.

Jenerette, G.D., Harlan, S.L., Buyantuev, A., Stefanov, W.L., Declet-Barreto, J., Ruddell, B.L., Myint, S.W., Kaplan, S., Li, X., 2016. Micro-scale urban surface temperatures are related to land-cover features and residential heat related health impacts in Phoenix, AZ USA. Landscape Ecol. 31 (4), 745–760.

Jiang, S., Zhou, J., Qiu, S., 2022. Digital agriculture and urbanization: mechanism and empirical research. Technol. Forecasting Social Change 180 (March 2021), 121724. https://doi.org/10.1016/j.techfore.2022.121724.

Johnson, D.P., Stanforth, A., Lulla, V., Luber, G., 2012. Developing an applied extreme heat vulnerability index utilizing socioeconomic and environmental data. Appl. Geogr. 35, 23–31. https://doi.org/10.1016/j.apgeog.2012.04.006.

Jones, H.G., Vaughan, R.A., 2010. Remote Sensing of Vegetation: Principles, Techniques, and Applications. Oxford University Press, New York, p. 353.

Kafy, A.-A., Faisal, A.-A., Al Rakib, A., Roy, S., Ferdousi, J., Raikwar, V., Kona, M.A., Fatin, S.M.A.A., 2021. Predicting changes in land use/land cover and seasonal land surface temperature using multi-temporal landsat images in the northwest region of Bangladesh. Heliyon 7 (7), e07623.

Kane, S.N., Mishra, A., Dutta, A.K., 2016. Preface: International Conference on Recent Trends in Physics (ICRTP 2016). J. Phys. Conf. Ser. 755. doi: 10.1088/1742-6596/755/1/011001.

Kavzoglu, T., Colkesen, I., 2009. A kernel functions analysis for support vector machines for land cover classification. Int. J. Appl. Earth Obs. Geoinf. 11, 352–359. https://doi.org/10.1016/j.jag.2009.06.002.

Kayaga, S.M., Amankwaa, E.F., Gough, K.V., Wilby, R.L., Abarike, M.A., Codjoe, S.N.A., Kasei, R., Nabilse, C.K., Yankson, P.W.K., Mensah, P., Abdullah, K., Griffiths, P., 2021. Cities and extreme weather events: impacts of flooding and extreme heat on water and electricity services in Ghana. Environ. Urban. 33, 131–150. https://doi.org/10.1177/0956247820952030.

Kim, S.W., Brown, R.D., 2021. Urban heat island (UHI) variations within a city boundary: a systematic literature review. Renew. Sustain. Energy Rev. 148, 111256 https://doi.org/10.1016/j.rser.2021.111256.

Krehbiel, C.P., Jackson, T., Henebry, G.M., 2016. Web-enabled landsat data time series for monitoring urban heat island impacts on land surface phenology. IEEE J. Sel. Top. Appl. Earth Obs. Remote Sens. 9, 2043–2050. https://doi.org/10.1109/JSTARS.2015.2496951.

Kumari, B., Shahfahad, Tayyab, M., Ahmed, I.A., Baig, M.R.I., Ali, M.A., Asif, Usmani, T. M., Rahman, A., 2021. Land use/land cover (LU/LC) change dynamics using indices overlay method in Gautam Buddha Nagar District-India. GeoJournal. doi: 10.1007/s10708-021-10374-w.

Li, J., Wang, Y., Ni, Z., Chen, S., Xia, B., 2020. An integrated strategy to improve the microclimate regulation of green-blue-grey infrastructures in specific urban forms. J. Clean. Prod. 271, 122555 https://doi.org/10.1016/j.jclepro.2020.122555.

Lin, Y., Jim, C.Y., Deng, J., Wang, Z., 2018. Urbanization effect on spatiotemporal thermal patterns and changes in Hangzhou (China). Build. Environ. 145, 166–176. https://doi.org/10.1016/j.buildenv.2018.09.020.

Liu, C.C., Lin, T.C., Yuan, K.Y., Chiueh, P.T., 2022. Spatio-temporal prediction and factor identification of urban air quality using support vector machine. Urban Clim. 41, 101055 https://doi.org/10.1016/j.uclim.2021.101055.

Malley, C.O., Piroozfar, P., Farr, E.R.P., Pomponi, F., 2015. Urban Heat Island (UHI) mitigating strategies: a case-based comparative analysis. Sustain. Cities Soc. 19, 222–235. https://doi.org/10.1016/j.scs.2015.05.009.

Mantey, S., Tagoe, N., Abaidoo, C., 2014. Estimation of land surface temperature and vegetation abundance relationship – a case study estimation of land surface temperature and vegetation. In: 3rd UMaT Bienn. Int. Min. Miner. Conf. 0–10.

Mantey, S., Tagoe, N.D., Abaidoo, C.A., 2014. Estimation of land surface temperature and vegetation abundance relationship – a case study. In: 3rd UMaT Biennial International Mining & Mineral Conference.

Meyers, J., Langston, A., Devereux, D., Lin, B., 2020. Mapping land surface temperatures and heat vulnerability in Darwin. CSIRO, Australia, City of Darwin.

Minu, S., Shetty, A., 2015. A comparative study of image change detection algorithms in MATLAB. Aquat. Procedia 4, 1366–1373. https://doi.org/10.1016/j.aqpro.2015.02.177.

Nangombe, S.S., Zhou, T., Zhang, W., Zou, L., Li, D., 2019. High-temperature extreme events over Africa under 1.5 and 2 °C of global warming. J. Geophys. Res. Atmos. 124 (8), 4413–4428.

Ning, J., Gao, Z., Meng, R., Xu, F., Gao, M., 2018. Analysis of relationships between land surface temperature and land use changes in the Yellow River Delta. Front. Earth Sci. 12 (2), 444–456.

Ningrum, W., 2018. Urban Heat Island towards Urban Climate. IOP Conf. Ser. Earth Environ. Sci. 118, 012048.

Nyamekye, C., Kwofie, S., Agyapong, E., Ofosu, S.A., Arthur, R., Appiah, L.B., 2021. Integrating support vector machine and cellular automata for modelling land cover change in the tropical rainforest under equatorial climate in Ghana. Curr. Res. Environ. Sustain. 3, 100052 https://doi.org/10.1016/j.crsust.2021.100052.

Oduro, C.Y., Adamtey, R., Ocloo, K., 2015. Urban growth and livelihood transformations on the fringes of African cities: a case study of changing livelihoods in Peri-Urban Accra. Environ. Nat. Resour. Res. 5, 81–98. https://doi.org/10.5539/enrr.v5n2p81.

Ojeh, V.N., Balogun, A.A., Okhimamhe, A.A., 2016. Urban-rural temperature differences in Lagos. Climate 4, 1–18. https://doi.org/10.3390/cli4020029.

Owusu, A.B., 2018. An assessment of urban vegetation abundance in Accra Metropolitan Area, Ghana: a geospatial approach. J. Environ. Geogr. 11, 37–44. https://doi.org/10.2478/jengeo-2018-0005.

Park, Y., Guldmann, J.M., Liu, D., 2021. Impacts of tree and building shades on the urban heat island: combining remote sensing, 3D digital city and spatial regression approaches. Comput. Environ. Urban Syst. 88, 15. https://doi.org/10.1016/j.compenvurbsys.2021.101655.

Pelta, R., Chudnovsky, A.A., 2017. Spatiotemporal estimation of air temperature patterns at the street level using high resolution satellite imagery. Sci. Total Environ. 579, 675–684. https://doi.org/10.1016/j.scitotenv.2016.11.042.

Puplampu, D.A., Boafo, Y.A., 2021. Exploring the impacts of urban expansion on green spaces availability and delivery of ecosystem services in the Accra metropolis. Environ. Challenges 5, 100283. https://doi.org/10.1016/j.envc.2021.100283.

Quan, Q., Liang, W., Yan, D., Lei, J., 2022. Influences of joint action of natural and social factors on atmospheric process of hydrological cycle in Inner Mongolia, China. Urban Clim. 41, 101043 https://doi.org/10.1016/j.uclim.2021.101043.

Ranagalage, M., Wang, R., Gunarathna, M.H.J.P., Dissanayake, D.M.S.L.B., Murayama, Y., Simwanda, M., 2019. Spatial forecasting of the landscape in rapidly urbanizing hill stations of South Asia: a case study of Nuwara Eliya, Sri Lanka (1996–2037). Remote Sens. 11 (15), 1743.

Ringard, J., Dieppois, B., Rome, S., Diedhiou, A., Pellarin, T., Konaré, A., Diawara, A., Konaté, D., Dje, B.K., Katiellou, G.L., Seidou Sanda, I., Hassane, B., Vischel, T., Garuma, G.F., Mengistu, G., Camara, M., Diongue, A., Gaye, A.T., Descroix, L., 2016. The intensification of thermal extremes in west Africa. Glob. Planet. Change 139, 66–77.

Rockström, J., Steffen, W., Noone, K., Persson, Å., Chapin, F.S., Lambin, E., Lenton, T.M., Scheffer, M., Folke, C., Schellnhuber, H.J., Nykvist, B., de Wit, C.A., Hughes, T., van der Leeuw, S., Rodhe, H., Sörlin, S., Snyder, P.K., Costanza, R., Svedin, U., Falkenmark, M., Karlberg, L., Corell, R.W., Fabry, V.J., Hansen, J., Walker, B., Liverman, D., Richardson, K., Crutzen, P., Foley, J., 2009. Planetary boundaries: exploring the safe operating space for humanity. Ecol. Soc. https://doi.org/10.5751/ES-03180-140232.

Roy, S., Pandit, S., Eva, E.A., Bagmar, M.S.H., Papia, M., Banik, L., Dube, T., Rahman, F., Razi, M.A., 2020. Examining the nexus between land surface temperature and urban growth in Chattogram Metropolitan Area of Bangladesh using long term Landsat series data. Urban Clim. 32, 100593 https://doi.org/10.1016/j.uclim.2020.100593.

Saha, S., Saha, A., Das, M., Saha, A., Sarkar, R., Das, A., 2021. Analyzing spatial relationship between land use/land cover (LULC) and land surface temperature (LST) of three urban agglomerations (UAs) of Eastern India. Remote Sens. Appl.: Soc. Environ. 22, 100507 https://doi.org/10.1016/j.rsase.2021.100507.

Shao, Y., Lunetta, R.S., 2012. Comparison of support vector machine, neural network, and CART algorithms for the land-cover classification using limited training data points. ISPRS J. Photogrammetry Remote Sensing 70, 78–87. https://doi.org/10.1016/j.isprsjprs.2012.04.001.

Simwanda, M., Ranagalage, M., Estoque, R.C., Murayama, Y., 2019. Spatial analysis of surface urban heat Islands in four rapidly growing african cities. Remote Sens. 11, 1–20. https://doi.org/10.3390/rs11141645.

Songsore, J., 2020. The urban transition in ghana: urbanization, national development and poverty reduction. Ghana Soc. Sci. J. 17, 120–172.

Songsore, J., McGranahan, G., 2012. Scaling Urban Environmental Challenges, Scaling Urban Environmental Challenges: From Local to Global and Back. Routledge. doi: 10.4324/9781849772471.

Songsore, J., Nabila, J.S., Yvon, Y., Avle, S., Bosque-Hamilton, E.K., Amponsah, P.E., OAlhassan, O., Satterthwaite, D., 2006. Environmental Health Watch and Disaster Monitoring in the Greater Accra Metropolitan Area (Gama), 2005. University of Ghana, Legon-Accra, Ghana.

Sun, D., Hu, C., Wang, Y., Wang, Z., Zhang, J., 2021. Examining spatio-temporal characteristics of urban heat islands and factors driving them in Hangzhou, China. IEEE J. Sel. Top. Appl. Earth Obs. Remote Sens. 14, 8316–8325. https://doi.org/10.1109/JSTARS.2021.3105586.

Tian, Y., Chen, C., Chen, X., Zhang, Q., Sun, R., 2020. Research on real-time analysis technology of urban land use based on support vector machine. Pattern Recogn. Lett. 133, 320–326. https://doi.org/10.1016/j.patrec.2020.03.022.

Tuffour-Mills, D., Antwi-Agyei, P., Addo-Fordjour, P., 2020. Trends and drivers of land cover changes in a tropical urban forest in Ghana. Trees, For. People 2, 100040. https://doi.org/10.1016/j.tfp.2020.100040.

UN-HABITAT, 2020. World Cities Report 2020; The Value of Sustainable Urbanization. doi: 10.18356/c41ab67e-en.

Vision, M., 1993. Image pre-processing 56–57.

Völker, S., Baumeister, H., Classen, T., Hornberg, C., Kistemann, T., 2013. Evidence for the temperature-mitigating capacity of urban blue space - a health geographic perspective. Erdkunde 67, 355–371. https://doi.org/10.3112/erdkunde.2013.04.05.

Wemegah, C.S., Yamba, E.I., Aryee, J.N.A., Sam, F., Amekudzi, L.K., 2020. Assessment of urban heat island warming in the greater accra region. Sci. African 8, e00426.

WHO, 2013. Protecting health from climate change: vulnerability and adaptation assessment. WHO Libr. Cat. Data.

Wilby, R.L., Kasei, R., Gough, K.V., Amankwaa, E.F., Abarike, M., Anderson, N.J., Codjoe, S.N.A., Griffiths, P., Kaba, C., Abdullah, K., Kayaga, S., Matthews, T., Mensah, P., Murphy, C., Yankson, P.W.K., 2021. Monitoring and moderating extreme indoor temperatures in low-income urban communities. Environ. Res. Lett. 16 (2), 024033.

Xu, L., Liu, X., Tong, D., Liu, Z., Yin, L., Zheng, W., 2022. Forecasting Urban Land Use Change Based on Cellular.

Xu, L., Liu, X., Tong, D., Liu, Z., Yin, L., Zheng, W., 2022b. Forecasting urban land use change based on cellular automata and the PLUS model. Land 11, 652. https://doi.org/10.3390/land11050652.

Yao, R., Wang, L., Huang, X., Sun, L., Chen, R., Wu, X., Zhang, W., Niu, Z., 2021. A robust method for filling the gaps in MODIS and VIIRS land surface temperature data. IEEE Trans. Geosci. Remote Sens. 59, 10738–10752. https://doi.org/10.1109/TGRS.2021.3053284.

Zhang, N., Chen, Y., Luo, L., Wang, Y., 2017. Effectiveness of different urban heat island mitigation methods and their regional impacts. Am. Meteorol. Soc. 18, 2991–3012. https://doi.org/10.1175/JHM-D-17-0049.1.

Zhang, Y., Odeh, I.O.A., Han, C., 2009. Bi-temporal characterization of land surface temperature in relation to impervious surface area, NDVI and NDBI, using a sub-pixel image analysis. Int. J. Appl. Earth Obs. Geoinf. 11 (4), 256–264.

Zhao, T., Shi, J., Entekhabi, D., Jackson, T.J., Hu, L., Peng, Z., Yao, P., Li, S., Kang, C.S., 2021. Retrievals of soil moisture and vegetation optical depth using a multi-channel collaborative algorithm. Remote Sens. Environ. 257, 112321 https://doi.org/10.1016/j.rse.2021.112321.

Zheng, Y., Tang, L., Wang, H., 2021. An improved approach for monitoring urban built-up areas by combining. J. Clean. Prod. 328, 129488 https://doi.org/10.1016/j.jclepro.2021.129488.

Zhou, D., Bonafoni, S., Zhang, L., Wang, R., 2018. Remote sensing of the urban heat island effect in a highly populated urban agglomeration area in East China. Sci. Total Environ. 628–629, 415–429. https://doi.org/10.1016/j.scitotenv.2018.02.074.